Effects of quantum decoherence in a future supernova neutrino detection

Marcos V. dos Santos,[1,*] Pedro C. de Holanda,[1,†] Pedro Dedin Neto,[1,2,‡] and Ernesto Kemp[1,3,§]

[1]*Universidade Estadual de Campinas, Instituto de Física Gleb Wataghin, R. Sérgio Buarque de Holanda, 777, Brazil*

[2]*Niels Bohr International Academy & DARK, Niels Bohr Institute, University of Copenhagen, Blegdamsvej 17, 2100 Copenhagen, Denmark*

[3]*Gran Sasso Science Institute-GSSI, Viale Francesco Crispi, 7 Rectorate, Via Michele Iacobucci, 2, 67100 L'Aquila, Italy*

(Received 11 July 2023; accepted 16 October 2023; published 17 November 2023)

Quantum decoherence effects in neutrinos, described by the open quantum systems formalism, serve as a gateway to explore potential new physics, including quantum gravity. Previous research extensively investigated these effects across various neutrino sources, imposing stringent constraints on the spontaneous loss of coherence. In this study, we demonstrate that even within the supernovae environment, where neutrinos are released as incoherent states, quantum decoherence could influence the flavor equipartition of 3ν mixing. Additionally, we examine the potential energy dependence of quantum decoherence parameters ($\Gamma = \Gamma_0(E/E_0)^n$) with different power laws ($n = 0, 2, 5/2$). Our findings indicate that future-generation detectors (DUNE, Hyper-K, and JUNO) can significantly constrain quantum decoherence effects under different scenarios. For a supernova located 10 kpc away from Earth, if no quantum decoherence is observed, DUNE could potentially establish 3σ bounds of $\Gamma \leq 6.2 \times 10^{-14}$ eV in the normal mass hierarchy (NH) scenario, while Hyper-K would impose a 2σ limit of $\Gamma \leq 3.6 \times 10^{-14}$ eV for the inverted mass hierarchy (IH) with $n = 0$—assuming no energy exchange between the neutrino subsystem and nonstandard environment. These limits become even more restrictive for a closer supernova. When we relax the assumption of energy exchange, for a 10 kpc distance, DUNE could establish a 3σ limit of $\Gamma_8 \leq 4.2 \times 10^{-28}$ eV for NH, while Hyper-K could constrain $\Gamma_8 \leq 1.3 \times 10^{-27}$ eV for IH ($n = 0$) with 2σ, which would be orders of magnitude stronger than the bounds reported to date. Furthermore, we examine the impact of neutrino loss during propagation for future supernova detection.

DOI: 10.1103/PhysRevD.108.103032

I. INTRODUCTION

Since the supernova SN1987A, the expectation for the next supernova (SN) neutrino detection has stimulated a number of works proposing tests on new physics in our Galaxy, making this event a promising natural laboratory for neutrino physics.

As approximately one Galactic SN is expected per century [1], the next event holds the opportunity to break through many aspects of neutrino physics, with capabilities of next-generation detectors, such as DUNE [2–4], Hyper-Kamiokande (HK) [5], and JUNO [6], leading to a sensitive future measurement, increasing the number of neutrino events from the current few dozen to tens of thousands or more in a SN explosion 10 kpc away from Earth. A typical core-collapse SN undergoes three main emission phases to be known (see [7] for a review): neutronization burst, where a high amount of ν_e is emitted given a rate of e^- capture in the first ∼30 ms after core bounce; accretion, where progenitor mass infall and a high luminosity are expected during roughly ∼1 s; and cooling, a thermal phase where a protoneutron star cools down via neutrino emission, with ∼10 s of duration.

With the possible future sensitivity and increasing sophistication in SN neutrino simulations [8–10], scenario of standard neutrino evolution until Earth is a matter of intense research. However, in an SN environment, collective oscillations led by $\nu - \nu$ interactions are a source of high uncertainties, since a definitive solution for the ν equation of motion has not been achieved, even with many ongoing developments in the topic [11]. One critical remark is that for the three mentioned SN emission phases, collective oscillations are expected to play an important role only in accretion and cooling, with no significant

*Corresponding author: mvsantos@ifi.unicamp.br
†holanda@ifi.unicamp.br
‡dedin@ifi.unicamp.br
§kemp@ifi.unicamp.br

impact on neutronization burst, given the large excess of ν_e over other flavors, turning it in a promising environment to test new physics.

Disregarding collective effects, it can be assumed that the only relevant neutrino conversion process is the Mikheyev-Smirnov-Wolfenstein (MSW) matter effect. Assuming an adiabatic propagation, the neutrino flux that comes out of the SN can be treated as an incoherent sum of mass states, and no oscillation is expected.[1] Since ν_α is generated as a mass state in matter ν_i^m, it leaves the SN as a mass state in vacuum ν_i until reaching Earth. Despite this expected incoherence, neutrinos coming from an SN could be affected by *quantum decoherence*. In this work, we show the impact of quantum decoherence, or the neutrino evolution from pure to mixed states given a coupling to the environment, in the case of a future SN neutrino detection.

There are different possible sources of decoherence in neutrino evolution, such as wave packet decoherence, that comes from different group velocities of neutrino mass states disentangling the respective wave packets [12–14], or even Gaussian averaged neutrino oscillation given by uncertainty in energy and path length [15]. The underlying physics in this work is of a different type and refers to effects induced by propagation in a nonstandard environment generated by beyond Standard Model physics, and the term *decoherence* used in this work refers to the latter.

The idea of inducing pure elementary quantum states into mixed ones was originally established by Hawking [16] and Bekenstein [17] and discussed by a number of subsequent works [18–22], being attributed to quantum (stochastic) fluctuations of space-time background given quantum gravity effects. Many authors have given a physical interpretation on the impact of such stochastic quantum gravitational background in neutrino oscillations [23–32], with expected decoherence being well described by open quantum systems formalism through the GKSL (Gorini–Kossakowski–Sudarshan–Lindblad) master equation. In particular, in [27], the authors provided a simple and interesting interpretation of physical scenarios for specific forms of the GKSL equation, and then we use a similar terminology in this work to guide our choices in the analysis.

Phenomenological studies designed to impose bounds on neutrino coupling to the environment through open quantum systems formalism were investigated in atmospheric [23,33,34], accelerator [35–43], reactor [43,44], and solar [33,45,46] neutrinos with different approaches. Only upper limits over quantum decoherence parameters were obtained up to now.

This paper is structured as follows: in Sec. II we show the quantum decoherence formalism, introducing the models to be investigated. In Sec. III we discuss the methods to factorize the neutrino evolution and how to use them to analyze the sensitivity to quantum decoherence in future SN detection. We also discuss the role of Earth matter effects. Our results are presented in Sec. IV, and in Sec. V we discuss how quantum decoherence could affect the neutrino mass ordering determination. Finally, in Sec. VI we present our conclusions.

[1]Given the indistinguishability of ν_μ and ν_τ ($\bar{\nu}_\mu$ and $\bar{\nu}_\tau$) in the detection, they are generally classified as ν_x ($\bar{\nu}_x$) in the literature.

II. QUANTUM DECOHERENCE EFFECTS IN SUPERNOVA NEUTRINOS

In this section, we devote ourselves to revisiting quantum decoherence formalism in neutrino mixing and show the impacts on the (already) incoherent SN neutrino fluxes.

A. Formalism

Considering the effects of quantum decoherence, we can write the GKSL equation in the propagation (mass) basis in vacuum [47,48],

$$\frac{d\rho}{dt} = -i[H,\rho] + \mathcal{D}(\rho), \tag{1}$$

where $\mathcal{D}(\rho) = \sum_p^{N^2-1}(V_p\rho V_p^\dagger - \frac{1}{2}\{V_p^\dagger V_p,\rho\})$ is a dissipation term, representing the neutrino subsystem coupling to the environment, with the density matrix defined as $\rho = \sum_i w_i|\psi_i\rangle\langle\psi_i|$, reduced to $\rho = |\psi\rangle\langle\psi|$ for a pure ensemble. If (1) is a general equation of motion to describe ν propagation and a nonstandard effect induces a non-null $\mathcal{D}(\rho)$, we require an increase of von Neumann entropy in the process, which can be achieved imposing $V_p = V_p^\dagger$ [49]. It is also possible to write the dissipation term on the rhs of (1) expanding it in the appropriated group generators as $\mathcal{D}(\rho) = \sum_a \mathcal{D}(\rho)_a\lambda_a = \sum_{a,b} D_{ab}\rho_b\lambda_a$, in which λ_a are the generators of SU(N) for a system of N neutrino families. In fact, the same procedure can be done in the Hamiltonian term of (1) in order to get a Lindbladian operator $\mathcal{L} = -2(\tilde{H} + \tilde{D})$, leading to

$$|\dot{\rho}\rangle = \mathcal{L}|\rho\rangle \tag{2a}$$

$$\mathcal{D}(\rho) = \sum_a \mathcal{D}(\rho)_a\lambda_a = \sum_{a,b} D_{ab}\rho_a\lambda_b \tag{2b}$$

$$H = \sum_a h_a\lambda_a = \sum_{a,b} H_{ab}\rho_a\lambda_b \tag{2c}$$

$$\rho = \sum_a \rho_a\lambda_a \tag{2d}$$

that operates in a "vectorized" density matrix $|\rho\rangle$ with dimension N^2 (where for $N = 3$ levels, the density matrix is defined as $|\rho\rangle = (\rho_0,\rho_1,\rho_2,\rho_3,\rho_4,\rho_5,\rho_6,\rho_7,\rho_8)^T$). In three neutrino mixing, as we can see, $|\rho\rangle$ has dimension nine and $\mathcal{L}$ is a 9×9 matrix. We use the notation $\tilde{D}$ and $\tilde{H}$ to refer to the respective matrices in this nine-dimensional

vector space, in contrast to $\mathcal{D}$ and H which are defined in a three-dimensional vector space. A general form of the Hamiltonian part $\tilde{H}$ for three neutrinos can be found in Appendix A.

One of the advantages of this formalism is that, despite a lack of understanding about the microscopic phenomena we are interested in modeling, we are able to infer the resulting damping effects by properly parametrizing $\mathcal{D}(\rho)$ (or more specifically $\tilde{D}$) in a generic way[2]:

$$\tilde{D} = -\begin{pmatrix} 0 & 0 & 0 & 0 & 0 & 0 & 0 & 0 & 0 \\ 0 & -\gamma_1 & \beta_{12} & \beta_{13} & \beta_{14} & \beta_{15} & \beta_{16} & \beta_{17} & \beta_{18} \\ 0 & \beta_{12} & -\gamma_2 & \beta_{23} & \beta_{24} & \beta_{25} & \beta_{26} & \beta_{27} & \beta_{28} \\ 0 & \beta_{13} & \beta_{23} & -\gamma_3 & \beta_{34} & \beta_{35} & \beta_{36} & \beta_{37} & \beta_{38} \\ 0 & \beta_{14} & \beta_{24} & \beta_{34} & -\gamma_4 & \beta_{45} & \beta_{46} & \beta_{47} & \beta_{48} \\ 0 & \beta_{15} & \beta_{25} & \beta_{35} & \beta_{45} & -\gamma_5 & \beta_{56} & \beta_{57} & \beta_{58} \\ 0 & \beta_{16} & \beta_{26} & \beta_{36} & \beta_{46} & \beta_{56} & -\gamma_6 & \beta_{67} & \beta_{68} \\ 0 & \beta_{17} & \beta_{27} & \beta_{37} & \beta_{47} & \beta_{57} & \beta_{67} & -\gamma_7 & \beta_{78} \\ 0 & \beta_{18} & \beta_{28} & \beta_{38} & \beta_{48} & \beta_{58} & \beta_{68} & \beta_{78} & -\gamma_8 \end{pmatrix} \tag{3}$$

in three neutrino mixing. Although it is not explicit, the entries in matrix (3) can be directly related to the coefficients of expansion of V_p in the generators of SU(3), or $\gamma, \beta = f(v_p)$, with v_p coming from $V_p = \sum_a v_{pa}\lambda_a$. Note that the null entries in the first column of (3) are given by the Hermiticity of V_p, which also enables rewriting the dissipation term as $\mathcal{D}(\rho) = \frac{1}{2}\sum_p^{N^2-1}[[V_p, \rho], V_p]$, showing that terms proportional to identity in the SU(3) expansion vanish, making the first row of (3) also null. It is important to note that the parameters used to define D_{ab} are not all independent. They are related to each other in order to ensure complete positivity, which is a necessary condition for a quantum state to be physically realizable [40,52,53] (see [40] for a set of relations in a three-level system).

However, it is not viable to investigate this general format of (3) given the number of parameters. Therefore, in this work, we restrict ourselves to cases in which $\tilde{D}$ is diagonal as in [45], in order to capture the effects of interest arising from quantum decoherence (QD). We tested a nondiagonal version of $\tilde{D}$ using complete positivity relations, and our results are not significantly affected.

In the context of supernova neutrinos, the neutrino propagates a large distance inside the supernova ($\sim 10^8$ km); then we also investigate the impact of QD combined with SN matter effects. A possible procedure to cross check it is by rotating Eq. (1) to flavor basis, where the Hamiltonian can be summed to an MSW potential, i.e., $H_f = H_f^{\text{vac}} + V_W$. However, as it will be more clear in Sec. III A, the probability we are interested in is between mass eigenstates on both matter and vacuum, which can be accomplished by diagonalizing the Hamiltonian in the flavor basis using a proper transformation.

B. Selected models

Since we analyze diagonal versions of (3), $\beta_{ab} = 0$ for all a and b. In works such as [45,54] it is shown that quantum decoherence can give rise to two disentangled effects when the evolution occurs in vacuum: the pure decoherence, where a coherent state becomes incoherent along propagation, and the relaxation effect, responsible to lead the ensemble to a maximal mixing. As decoherence effects on SN neutrinos are suppressed due to matter effects on the mixing angle and long propagation lengths,[3] we do not expect pure decoherence effects to play any role in the propagation, being only (possibly) affected by relaxation.

Up to this date, and to the authors' best knowledge, there is no consistent theory in which you can get the parameters of $\tilde{D}$ from quantum gravity, or address the possibility of energy-dependency of these parameters. Different works [23,27,33,55] suggested the possibility of a dependency on energy as $\gamma_i = \gamma_{0_i}(E/E_0)^n$ motivated by quantum spacetime phenomenology, where E_0 is an arbitrary energy scale. In this work, we chose $E_0 = 10$ MeV to match the energy scale of supernova neutrinos. As for the energy dependence, we explore the scenarios with $n = 0$ and $n = 2$, given that most of the works check these power law exponents for γ_i, which enables us to compare SN limits to other sources (and works), and $n = 5/2$, well-motivated by the natural Planck scale for the SN energy range of 0–100 MeV. By natural scale, we refer to $\gamma_{0_i} = \xi_{\text{Planck}}/M_{\text{Planck}}^{n-1}$ with $\xi_{\text{Planck}} \sim 1$ [27,56], making $\gamma_{0i} = \xi_{\text{Planck}} M_{\text{Planck}}^{1}$, $\xi_{\text{Planck}} M_{\text{Planck}}^{-1}$, and $\xi_{\text{Planck}} M_{\text{Planck}}^{-3/2}$ for our choices of $n = 0$, 2, and 5/2.

With dimensional analysis (which can be further justified when solving the evolution equation), we expect that the effects of decoherence would show up for distances larger than a *coherence length*, defined by $L_{\text{coh}} = 1/\gamma$. In Fig. 1 we show the expected coherence length for these values of n. We see that if this "natural" scale holds, $n = 0$ and 2 would be possibly ruled out by terrestrial and solar experiments, whereas for $n = 3$, L_{coh} is out of the observable Universe for the expected SN-ν energy scale. For the mentioned values of n, we analyze the following models.

[2]For some forms of $\mathcal{D}(\rho)$ derived from first principles, see [50,51].

[3]If neutrinos are only affected by the MSW effect, it is possible for ν_μ and ν_τ to oscillate to each other. It generally does not affect the analysis of flavor conversion, once they are indistinguishable in the detection, and therefore generally denoted as ν_x. However, as we will see in Sec. III, their creation in coherent states changes one of the tested QD models here.

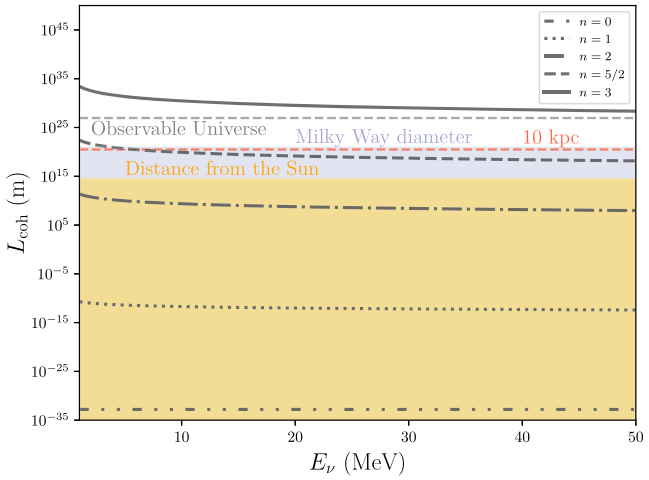

FIG. 1. Coherence length ($L_{\rm coh} = 1/\gamma$) for values of n in a power law of decoherence coefficients $\gamma = \gamma_0(E/E_0)^n$ for a "natural" scale of quantum gravity, with $\xi_{\rm Planck} = 1$. The yellow region corresponds to the solar system edge, while the blue region is the Milky Way diameter, and the dashed gray line represents the edge of the observable Universe.

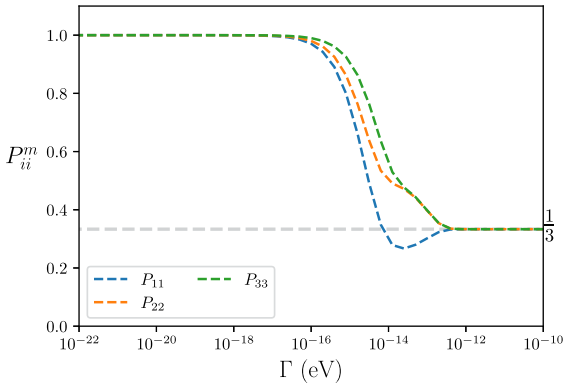

FIG. 2. Survival probabilities of state ν_i^m (mass state in matter basis) inside the SN for the MSC$^{\not\epsilon}$ model (no exchange of energy from neutrinos and environment in vacuum) and $n = 0$ (and then $\Gamma = \Gamma_0$). The SN matter density profile used is from a Garching simulation of a $40M_\odot$ (LS180-s40.0) progenitor [10,57], shown in Fig. 22 in Appendix B.

1. Mass state coupling (MSC)

The neutrino mass basis is coupled to the environment, and the relaxation effect leads to maximal mixing. In $3-\nu$ mixing, it means a $1/3$ probability of detecting any state. In this model, we test two possible scenarios related to energy conservation in the neutrino subsystem:

(i) MSC$^{\not\epsilon}$ ($[H, V_p] = 0$): Here, the neutrino energy is conserved, in the sense that no transition among the mass eigenstates is induced by the nonstandard vacuum.[4] It means that $V_p = \mathbf{v}_3\lambda_3 + \mathbf{v}_8\lambda_8$, where λ_a are Gell-Mann matrices and $\mathbf{v}_a = \sum_{p=1}^{8} v_{pa}$, with a ranging from 0 to 8 in the SU(3) expansion of V_p. To simplify the analysis we choose a diagonal version of the dissipation term in (3) with a single parameter Γ. Additionally, using complete positivity relations [40], we can find the special case of $\tilde{D} = \mathrm{diag}(0,\Gamma,\Gamma,0,\Gamma/4,\Gamma/4,\Gamma/4,\Gamma/4,0)$, with $\Gamma = \Gamma_0(E/10\ \mathrm{MeV})^n$. The transition probabilities amongst mass states in vacuum are null in this case. However, if we look at the propagation inside the supernova layers, in a diagonalized basis of the mass state in matter $P_{ij}^{m(\mathrm{SN})}$, this probability could be nonnull for $i \neq j$, i.e., transitions between ν_i^m and ν_j^m are allowed and would change proportionally to $e^{-\Gamma}$. Therefore, the coherence length to be investigated is the SN radius, and the matter effects in addition to quantum decoherence would induce a maximal mixing inside the SN. In Fig. 2 we show the transition probabilities of mass state in the matter basis calculated using the slab approach with a simulated SN density profile from the Garching group [10,57], corresponding to a progenitor of $40M_\odot$. More details about our solution are in Appendix B. When the neutrino is released to vacuum, it is no longer affected by quantum decoherence until detection. Since the length traveled inside the Earth by the neutrino is much smaller than $L_{\rm coh}^{\rm SN}$, we do not take the quantum decoherence in Earth matter into account in this specific case, albeit standard nonadiabatic MSW effect could play a role. Note that this regime essentially depends on ν matter effects in the SN.

(ii) MSC$^{\epsilon}$ ($[H, V_p] \neq 0$): In this model, we relax the above assumption, allowing some exchange of ν energy with the "nonstandard" environment. In this case, the energy exchange allows for the transition among the mass eigenstates, which have different well-defined energies. We have defined the most general version of a diagonal dissipation matrix as specified in (3): $\tilde{D} = \mathrm{diag}(0,\gamma_1,\gamma_2,\gamma_3,\gamma_4,\gamma_5,\gamma_6,\gamma_7,\gamma_8)$. In [27], this choice of $\tilde{D}$ is intrinsically related to the *mass state selected* scenario to be impacted by quantum gravitational effects. To quantify the effects of this model, we solve analytically (1) to get the probabilities of interest in the mass basis in vacuum[5]:

[4]In our notation, the superscript the symbol $\not\epsilon$ indicates that there is no exchange of energy with the environment, while ϵ has the opposite meaning.

[5]The expected (adiabatic MSW) solution for the probabilities is a Kronecker delta, i.e., $P_{ij} = \delta_{ij}$.

$$
\begin{aligned}
P_{11} &= \frac{1}{3} + \frac{1}{2}e^{-\gamma_3 x} + \frac{1}{6}e^{-\gamma_8 x} \\
P_{12} &= \frac{1}{3} - \frac{1}{2}e^{-\gamma_3 x} + \frac{1}{6}e^{-\gamma_8 x} \qquad P_{22} = P_{11} \\
P_{13} &= \frac{1}{3} - \frac{1}{3}e^{-\gamma_8 x} \qquad P_{23} = P_{13}, \\
P_{33} &= \frac{1}{3} + \frac{2}{3}e^{-\gamma_8 x}
\end{aligned} \tag{4}
$$

with x as the propagated distance. For other possible probabilities on this basis, we use $P_{ij} = P_{ji}$. It should be noted that on this basis the probabilities depend only on γ_3 and γ_8. The reason is that when solving the set of differential equations in (2), the equations corresponding to γ_3 and γ_8, i.e., $\mathcal{L}_{3b}$ and $\mathcal{L}_{8b}$ are the only decoupled ones, independent of Hamiltonian terms.

If we look at γ_i parameters in terms of $\mathbf{v}_a$ coefficients of the SU(3) expanded V_p we find

$$
\begin{aligned}
\gamma_3 &= \mathbf{v}_1^2 + \mathbf{v}_2^2 + \frac{\mathbf{v}_4^2}{4} + \frac{\mathbf{v}_5^2}{4} + \frac{\mathbf{v}_6^2}{4} + \frac{\mathbf{v}_7^2}{4} \\
\gamma_8 &= \frac{3\mathbf{v}_4^2}{4} + \frac{3\mathbf{v}_5^2}{4} + \frac{3\mathbf{v}_6^2}{4} + \frac{3\mathbf{v}_7^2}{4}.
\end{aligned} \tag{5}
$$

Equation (5) shows that γ_3 and γ_8 are not independent. In order to compare our results to solar limits [45], we can use the same notation to define

$$
\begin{aligned}
\Gamma_3 &= \mathbf{v}_1^2 + \mathbf{v}_2^2 \\
\Gamma_8 &= \frac{3\mathbf{v}_4^2}{4} + \frac{3\mathbf{v}_5^2}{4} + \frac{3\mathbf{v}_6^2}{4} + \frac{3\mathbf{v}_7^2}{4},
\end{aligned} \tag{6}
$$

leading to $\gamma_3 = \Gamma_3 + \Gamma_8/3$ and $\gamma_8 = \Gamma_8$, resulting in pure (independent) relaxation Γ parameters, that will be the ones effectively inducing the maximal admixture in this scenario. The energy dependence is explicitly written as $\Gamma_i = \Gamma_{0i}(E/10\ \mathrm{MeV})^n$ with $i = \{3, 8\}$. Note that the effective distance of this particular case is the total neutrino propagation, i.e., vacuum propagation is also affected, and it can be split into the regime in the SN and outside its surface until reaching the detector at Earth, $L = L^{\mathrm{SN}} + L^{\mathrm{Vac}}$. Similarly to *i*), we solve the probabilities associated with possible transitions in supernova layers only numerically. However, as we discuss in Sec. III A, given that $L^{\mathrm{Vac}} \gg L^{\mathrm{SN}}$, the approximation of $L \sim L^{\mathrm{Vac}}$ is assumed in our calculations.

2. Neutrino loss

As mentioned in [27], it is possible to have a scenario with neutrino loss, where neutrinos are captured by effects of quantum gravity during propagation, and re-emitted to a different direction, never reaching the detector at Earth. In this picture, the authors made a choice of $D_{00} \neq 0$. Looking at the most general form of $\mathcal{D}(\rho)$, it is possible to say that this choice is completely out of open quantum systems formalism, i.e., naturally $\mathcal{D}(\rho)_{0b} = 0$ when the master equation (1) is assumed to describe the evolution of the reduced quantum system, with trace preserving all times. Even though, to explore such an interesting physical situation, we test this nonunitary case that matches the choice $\gamma_i = \gamma$ with i from 1 to 8, then $\tilde{D} = -\mathrm{diag}(\gamma, \gamma, \gamma, \gamma, \gamma, \gamma, \gamma, \gamma)$, with $\gamma = \gamma_0(E/10\ \mathrm{MeV})^n$. The solution of (1) gives

$$
\begin{aligned}
P_{ii} &= e^{-\gamma x} \\
P_{ij} &= 0
\end{aligned} \tag{7}
$$

for any i, j from 1 to 3 with $i \neq j$. Note that in this result, in contradiction to conventional unitary models, one state does not go to another, i.e., $\sum_i P_{ij} \neq 1$, once neutrinos are lost along the way.

In the solutions of the equation of motion shown above, we absorbed a factor of 2 in the quantum decoherence parameters, i.e., $-2\gamma_i \to -\gamma_i$, with no loss of generality, since what matters in our results is the intensity of a deviation from a standard scenario.

III. METHODOLOGY AND SIMULATION

To test the QD models discussed in the context of a future SN detection, we use the neutrino flux coming from supernovae simulations from the Garching group [10]. For MSC^{e} described in item *i*) of MSC in Sec. II B, we exploit a $40M_\odot$ progenitor simulation (LS180-s40.0) [57], since it has detailed matter density profiles, essential to explore such scenario. For all other cases investigated (MSC$^{\epsilon}$ and ν loss), we use simulations with $27M_\odot$ (LS220s27.0c) and $11.2M_\odot$ (LS220s11.2c) progenitor stars, detailed in [7].

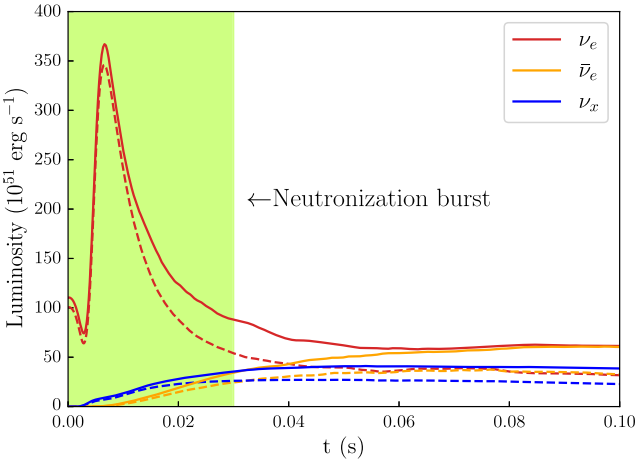

FIG. 3. Simulated ν luminosity for neutronization burst phase of the emission models of $27M_\odot$ (solid) and $11.2M_\odot$ (dashed) progenitor stars from the Garching group [7,10].

To avoid the large uncertainties of collective effects, we only use the flux from the neutronization burst phase (first 30 ms) in our analysis, in which effects induced by $\nu-\nu$ interaction are expected to not play a significant role. In Fig. 3 we show the luminosity of all flavors along the time window of this phase.

Next, we explain in more detail how to include non-standard physics of Eqs. (4) and (7) in SN neutrino evolution and our methods to use a future SN detection to impose limits on QD parameters.

A. Factorization of the dynamics

Our analysis only takes into account the MSW effect in the neutronization burst through the standard matter effect on ν mixing. To combine QD effects and MSW through the ν generation, propagation, crossing through Earth, and detection, it is possible to factorize the flavor probabilities as

$$P_{\alpha\beta} = \sum_{i,j,k=1}^{3} P_{\alpha i}^{m(\mathrm{SN})} P_{ij}^{m(\mathrm{SN})} P_{jk} P_{k\beta}^{m(\mathrm{Earth})}$$
$$\bar{P}_{\alpha\beta} = \sum_{i,j,k=1}^{3} \bar{P}_{\alpha i}^{m(\mathrm{SN})} \bar{P}_{ij}^{m(\mathrm{SN})} \bar{P}_{jk} \bar{P}_{k\beta}^{m(\mathrm{Earth})}, \tag{8}$$

where $P_{\alpha\beta}$ ($\bar{P}_{\alpha\beta}$) are the transition probabilities from flavor α to β. The meaning of each term in (8) can be summarized as follows: $P_{\alpha i}^{m(\mathrm{SN})}$ is the probability of creating a ν_α as a i state in matter ν_i^m; $P_{ij}^{m(\mathrm{SN})}$ is the probability of converting $\nu_i^m \to \nu_j^m$ inside supernova layers; P_{jk} is the probability of converting $\nu_j \to \nu_k$ during propagation in vacuum until Earth; and by the end, $P_{k\beta}^{m(\mathrm{Earth})}$ is the probability of detecting a ν_β given a ν_k state considering (or not) Earth matter effects. The index m indicates that the creation or propagation is in matter. It is worth remembering that ν_e and $\bar{\nu}_e$ are created as a single mass eigenstate in matter. In this scenario, the sum over i vanishes, since we have $P_{ei}^{m(\mathrm{SN})} = \delta_{i3}$ and $\bar{P}_{ei}^{m(\mathrm{SN})} = \delta_{i1}$ for normal mass hierarchy (NH), and $P_{ei}^{m(\mathrm{SN})} = \delta_{i2}$ and $\bar{P}_{ei}^{m(\mathrm{SN})} = \delta_{i3}$ for inverted mass hierarchy (IH). As for ν_x, although it is created in a coherent superposition of the other two mass eigenstates, the interference phase would be averaged out, and therefore Eq. (8) is valid. In the context of a SN flux conservation, the simplest flavor conversion scheme could be described by just P_{ee} and $\bar{P}_{ee}$, and in standard neutrino mixing, the factorized probabilities in (8) become $P_{ij}^{m(\mathrm{SN})} = \delta_{ij}$, $P_{jk} = \delta_{jk}$ and $\bar{P}_{ij}^{m(\mathrm{SN})} = \delta_{ij}$, $\bar{P}_{jk} = \delta_{jk}$ for adiabatic evolution. Such a scenario can be changed by quantum decoherence, allowing for the conversion among mass eigenstates in vacuum and matter.

One can also note in (4), (5), (6), and (8) that for the MSC$^\epsilon$ model, P_{ee} is a function of Γ_3 and Γ_8 in IH but only of Γ_8 for NH. The $\bar{P}_{ee}$ has the opposite dependency, and we can write

$$P_{ee}^{\mathrm{IH}} = P_{ee}^{\mathrm{IH}}(\Gamma_3,\Gamma_8); \qquad P_{ee}^{\mathrm{NH}} = P_{ee}^{\mathrm{NH}}(\Gamma_8)$$
$$\bar{P}_{ee}^{\mathrm{IH}} = \bar{P}_{ee}^{\mathrm{IH}}(\Gamma_3); \qquad \bar{P}_{ee}^{\mathrm{NH}} = \bar{P}_{ee}^{\mathrm{NH}}(\Gamma_3,\Gamma_8).$$

These remarks on the survival probabilities of ν_e and $\bar{\nu}_e$ are essential in our results, once the flavor conversion of MSC can be described using uniquely P_{ee} and $\bar{P}_{ee}$.

Particularly for the MSC$^\varepsilon$ case, considering the propagation along supernova layers, $P_{ij}^{m(\mathrm{SN})}$ and $\bar{P}_{ij}^{m(\mathrm{SN})}$ will be affected by QD; nevertheless $P_{jk} = \delta_{jk}$ and $\bar{P}_{jk} = \delta_{jk}$, since with no exchange of energy to the environment, quantum decoherence would not play any role in the vacuum propagation. On the other hand, for MSC$^\epsilon$, both SN matter and vacuum would affect the neutrino mixing. However, as shown in Fig. 23 in Appendix B, a $\Gamma_{3,8} \gtrsim 10^{-18}$ eV or even beyond would be needed to have significant changes over $P_{ij}^{m(\mathrm{SN})}$. As it will be clear in Sec. IV, this value is much higher than the possible sensitivity of a future SN detection with only vacuum effects (given the large coherence length between the SN and Earth); then we take $P_{ij}^{m(\mathrm{SN})}$ and $\bar{P}_{ij}^{m(\mathrm{SN})}$ as δ_{ij} for MSC$^\epsilon$ from now on.

In order to check the sensitivity to QD parameters, we statistically analyze it in two scenarios: without Earth matter effects in neutrino (antineutrino) propagation, or $P_{ke}^{m(\mathrm{Earth})} = P_{ke}$ ($\bar{P}_{ke}^{m(\mathrm{Earth})} = \bar{P}_{ke}$) in (8); and then we check how Earth matter effects would impact our results.

Figure 4 shows both scenarios of P_{ee} and $\bar{P}_{ee}$ as a function of quantum decoherence parameters for neutrinos and antineutrinos, where neutrino hierarchy plays a relevant role in the considered scenarios. It is possible to see that Earth regeneration could enhance or decrease the sensitivity of standard physics on QD parameters for very specific energies and zenith angles θ_z. However, as we will see later, regeneration becomes more relevant for higher energies, generally at the end of the SN-ν simulated spectrum, limiting its impact on SN flavor conversion.

It is worth mentioning that for the MSC model, we expect asymptotically more sensitivity on P_{ee} in NH than IH, since for IH the standard probability is about the maximal admixture (1/3). In contrast, for $\bar{P}_{ee}$, both hierarchy scenarios are almost equally sensitive to a maximal admixture scenario. In the case of ν loss we see the opposite picture for P_{ee}, i.e., IH would be more impacted by an asymptotically null probability, and for $\bar{P}_{ee}$, NH would be highly affected, with low impact on IH.

As we will see later, the most general scheme of SN-ν fluxes at Earth cannot be parametrized with just P_{ee} and $\bar{P}_{ee}$ for the ν-loss scenario, given no conservation of total flux. Therefore it is needed to work out $P_{\alpha\beta}$ also for $\alpha,\beta = \mu,\tau$ (not shown in Fig. 4 for simplicity). We clarify it in the next section.

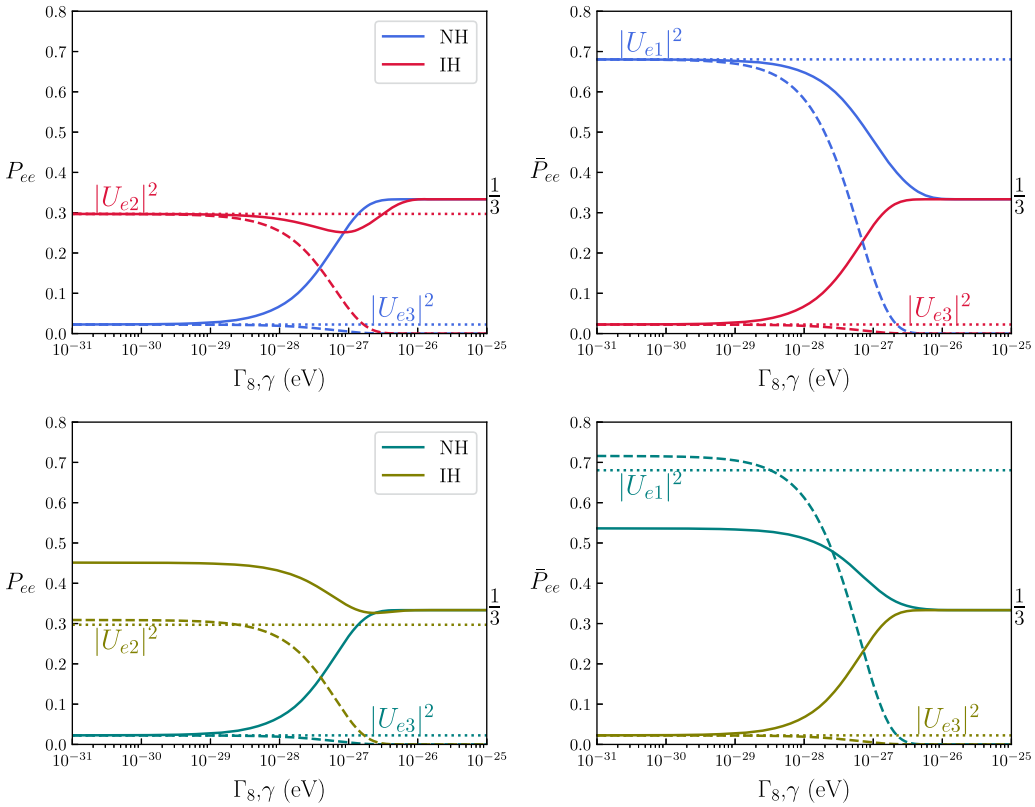

FIG. 4. Survivor probability for electron neutrinos (left) and antineutrinos (right) as a function of decoherence parameters for $n = 0$ (energy independent) and a 10 kpc propagation, without (upper plots) and with (down plots) Earth matter effects. Solid lines represent MSC^e scenario (Γ_8) with $\Gamma_3 = 10^{-27}$ eV and the dashed, the neutrino loss (γ). For the upper plots, quantum decoherence is taken into account only in vacuum in between SN surface until detection at Earth, with no regeneration considered. In the down ones, we set the zenith angle of $\theta_z = 180°$ and $E_\nu = 30$ MeV.

B. Exploring a future SN-ν detection

Since the detection of SN1987A through neutrinos, a Galactic SN is expected by the community as a powerful natural ν laboratory. The SN1987A neutrino detection greatly impacted what we know about SN physics, but the low statistics of the available data make predictions on standard ν admixture extremely challenging. On the other hand, the next generation of neutrino detectors promises a precise measurement of a Galactic SN, highly increasing our knowledge of SN-ν flavor conversion, with different detector technologies and capabilities. Here, we show the sensitivity of DUNE, HK, and JUNO on QD. These detectors have the following properties:

(a) DUNE will be a 40 kt Liquid-Argon TPC in the USA. We consider only the most promising detection channel $\nu_e + \mathrm{Ar} \to e^- + K^+$ [4] in our analysis, being sensitive to electron neutrinos and consequently to most neutronization burst flux.[6] We set an energy threshold to $E_{\mathrm{th}} = 4.5$ MeV and use the most conservative reconstruction efficiency reported in [4].

(b) Hyper-Kamiokande will be a water Cherenkov detector in Japan with a fiducial mass of ∼374 kt with the main detector channel as the inverse beta decay (IBD), sensitive to electron antineutrinos: $\bar{\nu}_e + p \to e^+ + n$ [5]. Also expected are several events from elastic scattering with electrons, with the advantage of sensitivity to all flavors: $\nu + e^- \to \nu + e^-$. We consider both channels in our analysis. We set a 60% overall detector efficiency and $E_{\mathrm{th}} = 3$ MeV [5].

(c) JUNO will be a liquid scintillator detector with a fiducial mass of 17 kt situated in China [58]. Despite the interesting multichannel detection technology reported by the collaboration, we take into account only IBD events. We set an overall efficiency of 50% and $E_{\mathrm{th}} = 3$ MeV in our analysis.

In order to compare the examined scenarios, we will consider only the energy information, calculating the number of events in the j-th energy bin as

$$N_j = n_d^c \int_0^\infty dt \int_0^\infty dE_\nu \frac{d^2\phi_\nu}{dt dE_\nu} \eta(E_\nu) \times \int_{E_i}^{E_f} d\bar{E}_\nu R_j(\bar{E}_\nu, E_\nu)\sigma(E_\nu), \quad (9)$$

[6]Actually, it depends on the neutrino mass hierarchy, once for MSW-NH the ν_e flux is highly suppressed.

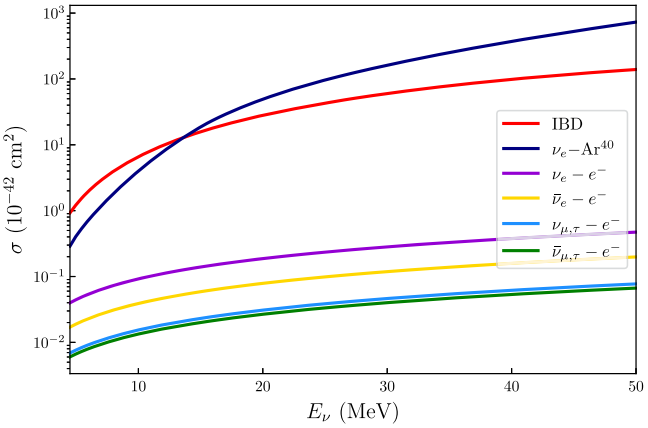

FIG. 5. ν total cross sections for IBD [59], ν_e – Ar charge current interaction (from SNOwGLoBES) [60], and elastic $\nu - e^-$ interaction [61].

where E_ν ($\bar{E}_\nu$) is the true (reconstructed) neutrino energy, n_d^c is the number of targets for each detector d, with c accounting for each specific channel, ϕ_ν is the neutrino flux, $\eta(E_\nu)$ is the efficiency that can eventually depend on ν energy, σ is the neutrino cross section (with each channel shown in Fig. 5), and R_j is the detector resolution.

We analyze the ν energy from the threshold of each detector up to 60 MeV. The ν mixing is encoded in the flux ϕ_ν, that can be written as

$$\begin{aligned}\phi_{\nu_e} &= \phi^0_{\nu_e} P_{ee} + \phi^0_{\nu_x}(1 - P_{ee}) \\ \phi_{\bar{\nu}_e} &= \phi^0_{\bar{\nu}_e} \bar{P}_{ee} + \phi^0_{\nu_x}(1 - \bar{P}_{ee}) \\ \phi_{\nu_x} &= \phi^0_{\nu_e}(1 - P_{ee}) + \phi^0_{\nu_x}(2 + P_{ee} + \bar{P}_{ee}) + \phi^0_{\bar{\nu}_e}(1 - \bar{P}_{ee})\end{aligned} \tag{10}$$

for the standard MSW (widely found in literature, see [7,62] for a review), where $\phi^0_{\nu_\alpha}$ refers to initial SN neutrino fluxes, and nonstandard QD effects are hidden in P_{ee} and $\bar{P}_{ee}$. In Fig. 6, the expected number of events for the three detectors are reported in the energy spectrum of simulated progenitors ($11.2M_\odot$ and $27M_\odot$) for both hierarchies and are compared to MSC$^\epsilon$ model. The results translate what is shown in Fig. 4, weighted by detector capabilities. Expected changes in the spectrum look more prominent when NH is assumed as a standard solution for DUNE, with an increase of ν_e events for both hierarchies. On the other hand, for HK and JUNO the MSC$^\epsilon$ effect results in a decrease of events in IH and an increase in NH, and it is not so clear which hierarchy would be more sensitive to the MSC$^\epsilon$ effect, since the number of QD parameters for each one is different for both P_{ee} and $\bar{P}_{ee}$. For instance, for $\bar{P}^{\rm NH}_{ee}$, fixing Γ_3, an increase in Γ_8 is weighted by the factor $1/3$ in the exponential terms, while $\bar{P}^{\rm IH}_{ee}$ is more sensitive to Γ_8, since the same change is multiplied by a factor of 1, but it is also independent of Γ_3. Note that Eq. (10) is valid for a conserved total flux, which does not remain in the ν-loss scenario. To get around this issue we propose a more generalized form of (10)

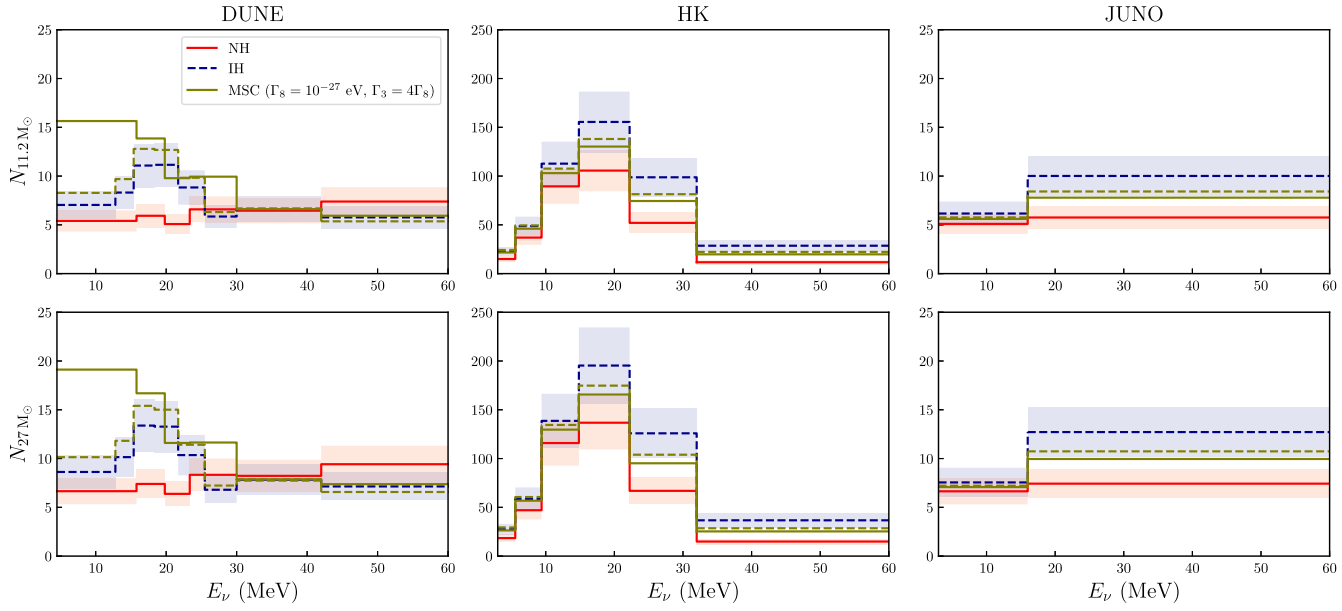

FIG. 6. Spectrum of events for DUNE, HK, and JUNO for NH (solid lines) and IH (dashed), with $n = 0$ for a 10 kpc SN with $11.2M_\odot$ and $27M_\odot$ progenitor mass simulations. Each column concerns a detector, while the rows are related to progenitor masses. The size of bins is at least twice the resolution at the specific energy and given a minimum threshold in the number of events per bin established in our analysis. The bands are to respect the 40% of the uncertainty of the flux over standard NH and IH, with details in the text. For the QD parameters, we used the values $\Gamma_8 = 10^{-27}$ eV and $\Gamma_3 = 4\Gamma_8$.

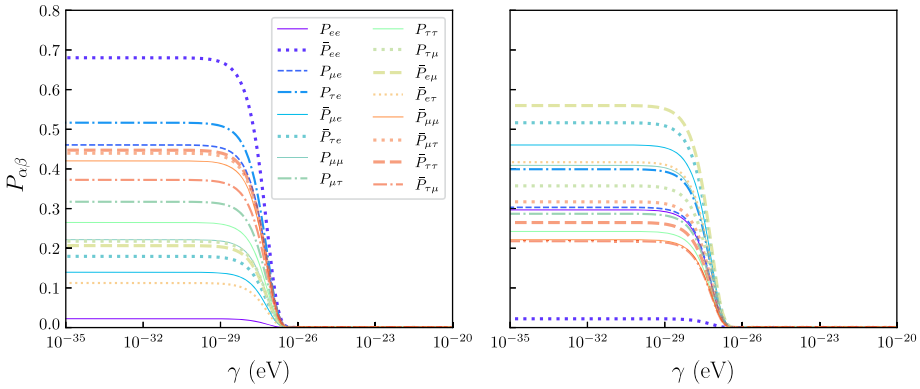

FIG. 7. Probabilities with the impact of ν-loss with $n = 0$ considering a 10 kpc SN for NH (left) and IH (right).

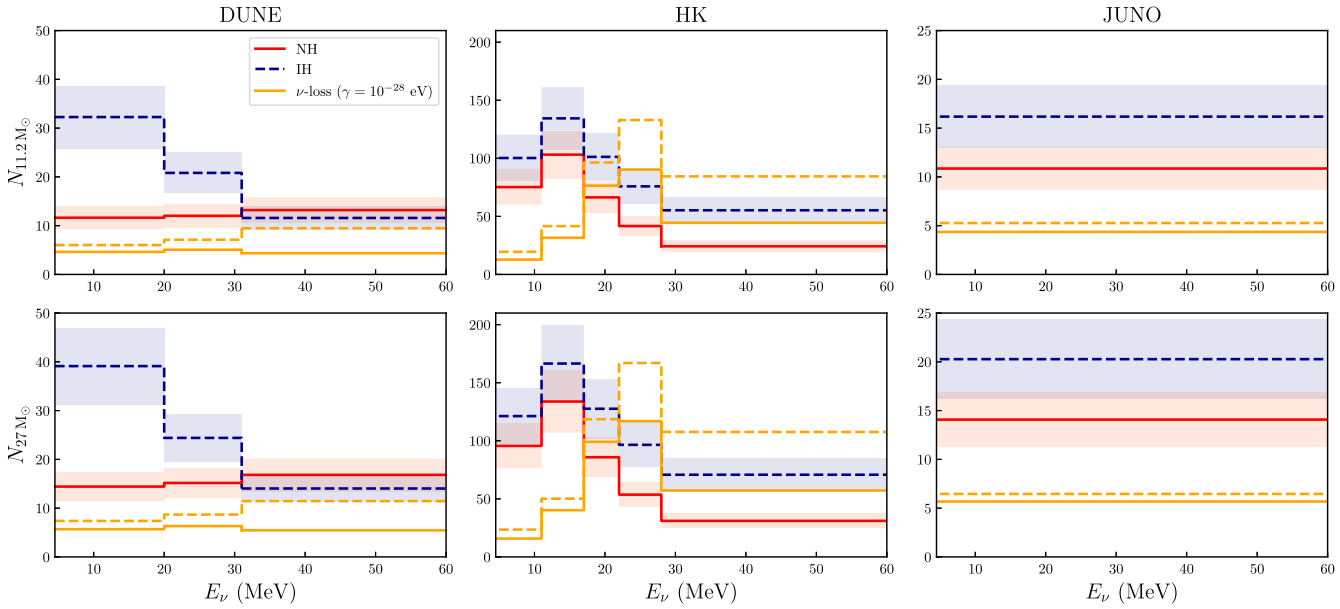

FIG. 8. Spectrum of events for DUNE, HK, and JUNO for NH (solid lines) and IH (dashed) compared to ν-loss model, with $n = 0$ for a 10 kpc SN with $11.2M_\odot$ and $27M_\odot$ progenitor mass simulations. For ν loss we use different bin sizes in order to achieve the requirement of the minimum number of events per bin of ~5. Given the lack of events in this scenario, we decided to use a single bin for JUNO.

$$
\begin{aligned}
\phi_{\nu_e} &= \phi^0_{\nu_e} P_{ee} + \phi^0_{\nu_x}(P_{\mu e} + P_{\tau e}) \\
\phi_{\bar{\nu}_e} &= \phi^0_{\bar{\nu}_e} \bar{P}_{ee} + \phi^0_{\nu_x}(\bar{P}_{\mu e} + \bar{P}_{\tau e}) \\
\phi'_{\nu_x} &= \phi^0_{\nu_e}(P_{e\mu} + P_{e\tau}) + \phi^0_{\nu_x}(P_{\mu\mu} + P_{\mu\tau} + P_{\tau\tau} + P_{\tau\mu}) \\
\phi'_{\bar{\nu}_x} &= \phi^0_{\bar{\nu}_e}(\bar{P}_{e\mu} + \bar{P}_{e\tau}) + \phi^0_{\bar{\nu}_x}(\bar{P}_{\mu\mu} + \bar{P}_{\mu\tau} + \bar{P}_{\tau\tau} + \bar{P}_{\tau\mu}) \\
\phi_{\nu_x} &= \phi'_{\nu_x} + \phi'_{\bar{\nu}_x},
\end{aligned}
\tag{11}
$$

where each probability can be factorized as described in (8). For the ones where $\alpha = \mu, \tau$, since these flavors are generated in a superposition of mass states in matter, the $\nu_\mu - \nu_\tau$ mixing should be taken into account, where $P^{m\mathrm{SN}}_{\alpha i}$ and $\bar{P}^{m\mathrm{SN}}_{\alpha i}$ would correspond to the proper square module of elements from the $U_{\mu\tau}$ mixing matrix.[7] In Fig. 7 we show each probability $P_{\alpha\beta}$ for a 10 kpc SN for the ν-loss scenario. In Fig. 8 we show the expected spectrum of events for the ν-loss model.

C. Role of Earth matter effects

Since a Galactic SN detection can be impacted by Earth matter effects, we also calculate P_{ee} and $\bar{P}_{ee}$ to each detector given the position of the SN in the sky.

[7]In the $\mu - \tau$ sector, such probability is associated to θ_{23} mixing, being a submatrix of U_{23} in the conventional PMNS decomposition. We also assume in this formula that any oscillation term is averaged out.

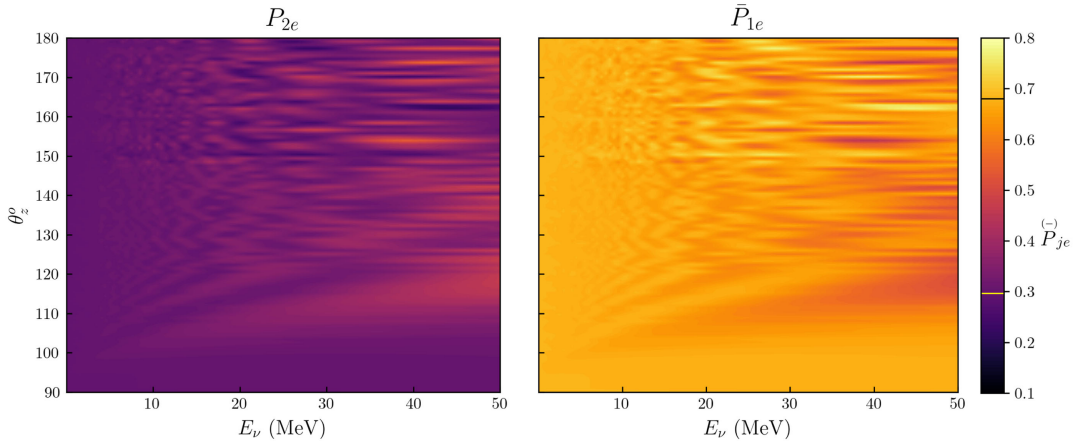

FIG. 9. P_{2e} (left) and $\bar{P}_{1e}$ (right) under Earth matter effects as a function of neutrino energy and zenith angle. In standard MSW in supernova mixing, P_{2e} and $\bar{P}_{1e}$ can be used to calculate the survival probabilities of ν_e (IH) and $\bar{\nu}_e$ (NH) respectively. The lines on the color bar are the adiabatic solutions for P_{2e} (yellow) and $\bar{P}_{1e}$ (black) without regeneration effects.

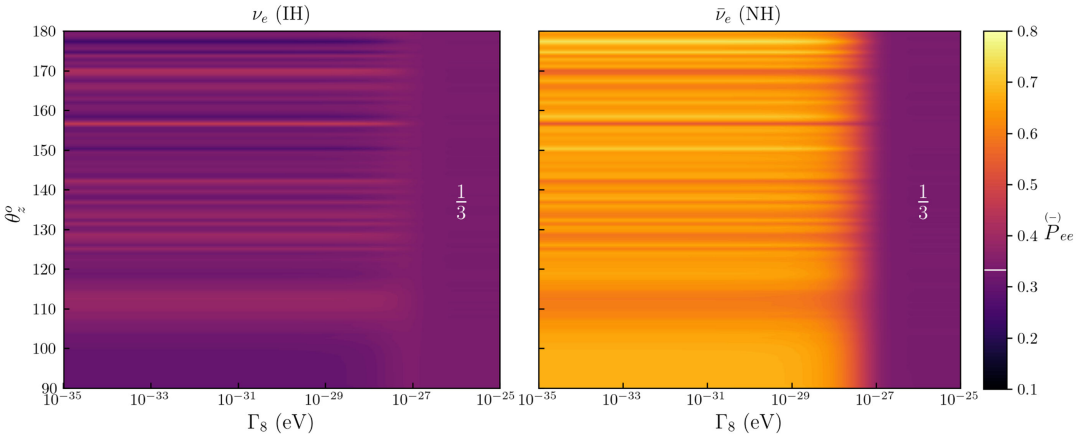

FIG. 10. P_{ee} in IH (left) and $\bar{P}_{ee}$ in NH (right) under Earth matter effects as a function of the QD parameter for $E_\nu = 30$ MeV, considering a SN 10 kpc away from Earth and $n = 0$. It is possible to see that QD suppresses regeneration effects for $\Gamma_8 \gtrsim 10^{-27}$ eV, where $\Gamma_3 = 10^{-32}$ eV was set. The white line on the color bar represents maximal mixing.

However, as shown in [63], it is not expected to play an important role in the neutronization burst. The reason is that regeneration would start to be important beyond $E_\nu \gtrsim 50$ MeV or even higher energies, which is close to the end of the expected spectrum. In Fig. 9 we show the impact of Earth matter effects in P_{ee} for a SN flux of ν_e in IH and $\bar{P}_{ee}$ for $\bar{\nu}_e$ in NH in a range of zenith angles for only nonadiabatic MSW effect (no quantum decoherence effects) using the PREM density profile available in [64], where 90° is a horizon of an observer at Earth (with no matter effects) and 180° represents a propagation all along Earth's diameter. Note that for P_{ee} in NH and $\bar{P}_{ee}$ in IH, regeneration does not play an important role.

In Fig. 10 we also see the QD effects (MSC$^\epsilon$ with $n = 0$) combined with Earth matter effects for a specific energy (similarly as shown in Fig. 4, but for a wide range of θ_z and the QD parameter). The asymptotic maximal mixing suppresses regeneration effects beyond $\Gamma_8 \sim 10^{-27}$ eV, being a leading effect. Since regeneration is a second-order effect, we will first analyze the sensitivity to QD in the next section without considering Earth matter effects, and by the end of Sec. IV B, we show its impact on the results.

IV. FUTURE LIMITS ON QUANTUM DECOHERENCE

In order to analyze the sensitivity to QD effects using simulated data, we perform a binned χ^2 through the pull method [65] over QD parameters for MSC and ν-loss scenarios:

$$\chi^2 = \sum_d \sum_{j=1}^{m} \frac{(N_{j,d}^{\text{true}} - (1+a)N_{j,d}^{\text{th}})^2}{N_{j,d}^{\text{th}}} + \frac{a^2}{\sigma_a^2}, \qquad (12)$$

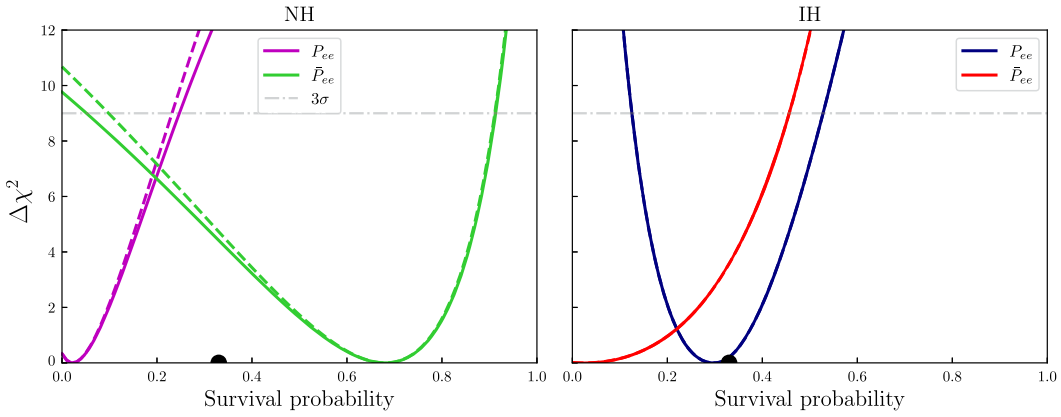

FIG. 11. Limits on P_{ee} and $\bar{P}_{ee}$ for the $27M_\odot$ (solid) and $11.2M_\odot$ (dashed) progenitor stars from simulations, considering only the neutronization burst. No quantum decoherence effects are taken into account in this figure. The distance from Earth considered was 10 kpc. The probability is assumed to be a free parameter as recently proposed in [67]. The assumption of a standard adiabatic MSW conversion at the SN is taken into account (as all along the article), getting rid of the energy dependency on P_{ee} and $\bar{P}_{ee}$. The black dot is the maximal mixing scenario (1/3). Note that the $11.2M_\odot$ line for IH matches to the $27M_\odot$, showing that the sensitivity for simulated progenitors tested is similar.

where m indicates the number of energy bins, d represents each detector, $N_{j,d}^{\text{true}}$ represents events predicted by the MSW solution, and $N_{j,d}^{\text{th}}$ accounts for the theoretical number of events of the marginalized model in our analysis, i.e., MSW + quantum decoherence respectively and the second term on the right-hand side take our estimation in the flux uncertainties of 40% into account [66]. In this context, we measure the statistical difference of a scenario with and without QD quantified by the χ^2 method.

We can note in Fig. 7 that since all probabilities vanish for high values of γ, $N \to 0$ for ν-loss. However in order to avoid a bias in our analysis, we marginalize over γ only in a range where the requirement of at least ~5 events per bin is achieved (we use the same rule for MSC). We also take the size of the bins to be twice the detector energy resolution. Using these requirements, JUNO allows a single bin for ν-loss, being a counting experiment for this analysis. The bins scheme for DUNE and HK are also changed for ν-loss compared with MSC in order to match the established minimum number of events per bin in the tested range of γ.

Before calculating the sensitivity on MSC and ν-loss with Eq. (12), we can treat P_{ee} and $\bar{P}_{ee}$ as free parameters, which is a reasonable approximation to an adiabatic propagation at the SN, since these probabilities are energy independent (see [67] for a more detailed discussion in the context of SN1987A). We perform a marginalization with $\chi^2(P_{ee}, \bar{P}_{ee})$ in Eq. (12) to understand how far asymptotically QD scenarios are from the standard ν mixing and also see how sensitive a combined measurement (DUNE+HK+JUNO) could be, using uniquely the neutronization burst. Figure 11 shows how a 10 kpc SN can impose limits to P_{ee} and $\bar{P}_{ee}$, with NH and IH concerning the true MSW model. The black dot represents maximal mixing or the asymptotic limit of MSC, which is closer to the IH solution (given by the corresponding best-fit value) than NH for P_{ee}, but in an intermediary point of hierarchies with respect to $\bar{P}_{ee}$. In the ν-loss scenario it is not so clear from Fig. 11 which hierarchy would be more sensitive to this effect, given the presence of other probabilities, such as the ones in Fig. 7.

Using Eq. (12) and the procedures described in Secs. II and III, we treat QD parameters as free and perform a χ^2 analysis in order to check how statistically distinguishable the scenarios are with and without QD, and therefore, how one could impose limits in these parameters based on a nonobservation of QD effects in a future SN detection. Since nowadays the neutrino mass hierarchy is not established, we include both scenarios in our analysis.

We test both MSW-NH versus the marginalized MSW-NH + QD and also the MSW-IH versus the marginalized MSW-IH + QD in order to understand how restrictive future detectors will be. The results will show that if QD plays any role in SN neutrinos, both possible ν hierarchies could be affected.

A. MSC$^\epsilon$

For the MSC$^\epsilon$ model, we calculate $\sqrt{\Delta\chi^2}$ over the parameter Γ, where $\Delta\chi^2 = \chi^2 - \chi^2_{\text{min}}$ (since we are not including statistical and systematic uncertainties when producing the "true" data, we always have $\chi^2_{\text{min}} = 0$). The results for the three experiments are summarized in Fig. 12, where the true scenario is NH, and we marginalize over NH + QD. Note that the sensitivity to Γ is different for each SN distance, with lower distances being more restrictive.

Since the traveled distance inside the SN is a fixed feature, the only aspect that the SN distance from Earth contributes is the number of events detected. Following Fig. 12, the best performance in NH is for DUNE, where,

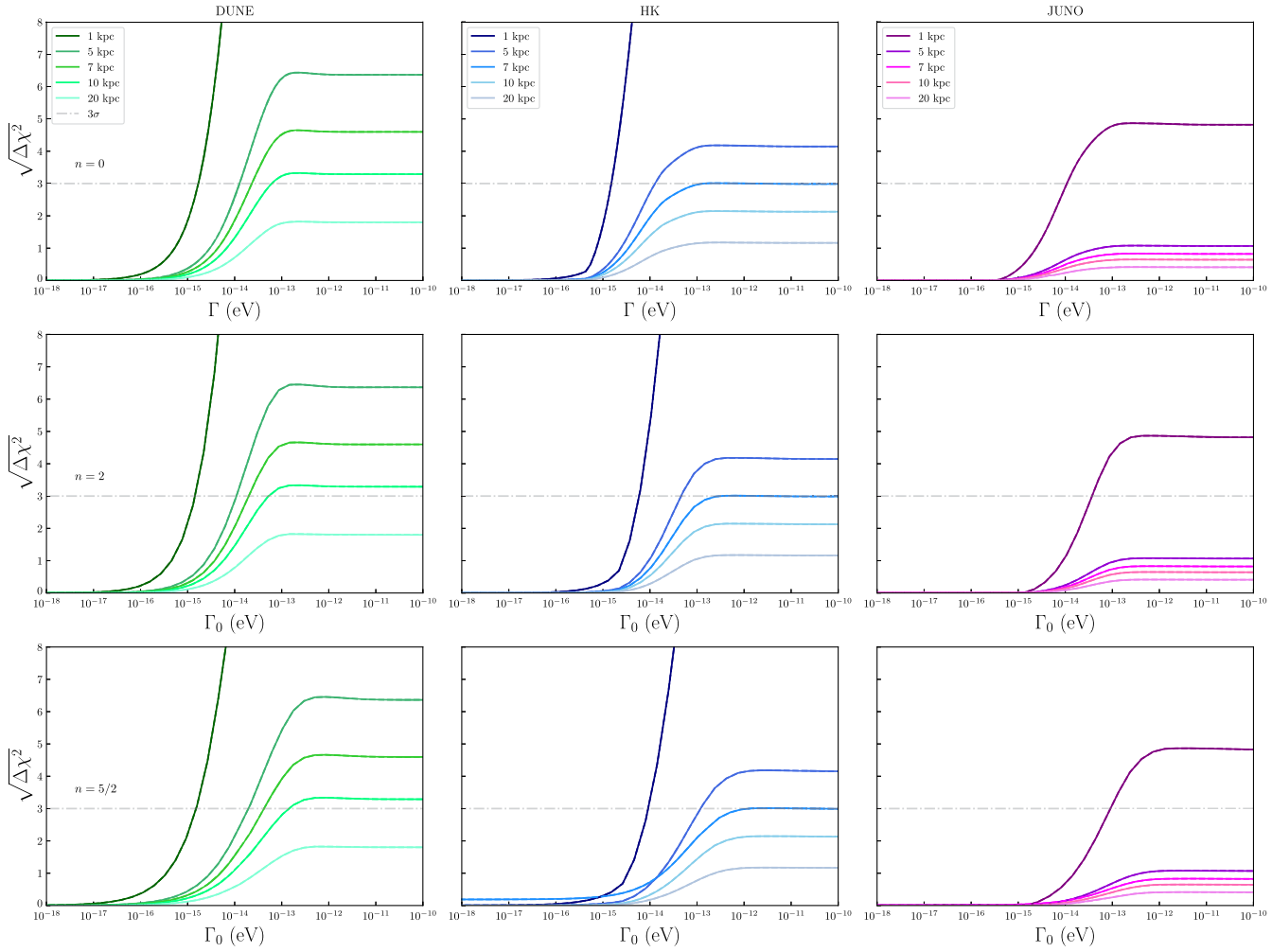

FIG. 12. Limits on Γ for various SN distances from Earth for DUNE (left), HK (middle), and JUNO (right) for the $40M_\odot$ progenitor star simulation. The true scenario taken into account was NH, and we marginalize the parameters over the theoretical NH + QD (MSC^e). No Earth matter effect was considered. Each row means a different value of n in the parametrization $\Gamma = \Gamma_0(E/E_0)^n$.

if no QD is observed, one could impose the following 3σ limits for a 10 kpc SN away from Earth:

$$\Gamma_0 \leq \begin{cases} 6.2 \times 10^{-14}\ \text{eV} & (n=0) \\ 5.2 \times 10^{-14}\ \text{eV} & (n=2) \\ 1.4 \times 10^{-13}\ \text{eV} & (n=5/2). \end{cases} \quad (13)$$

For a SN at a distance of 1 kpc, limits of $\mathcal{O}(10^{-16})$ eV can be reached. HK has also a good performance and achieves 2σ bounds for a 10 kpc SN. JUNO is not capable of individually achieving reasonable bounds on QD for SN distances $\gtrsim$1 kpc, but would also have a strong signal for a Galactic SN as close as 1 kpc away from Earth, which can be attributed to the small fiducial mass compared to HK and a single IBD channel considered in this work (with a significantly lower cross section than ν_e-Ar for energies above ∼15 MeV). Other channels, such as ν-p elastic scattering could possibly improve the results, but given the detection challenges associated, we decided to not include them here.

We also performed the same analysis using IH as the true theory and marginalizing over IH + QD. The results are shown in Fig. 13. The best performance is clearly for HK with a 2σ bound of

$$\Gamma_0 \leq \begin{cases} 3.6 \times 10^{-14}\ \text{eV} & (n=0) \\ 8.0 \times 10^{-14}\ \text{eV} & (n=2) \\ 2.4 \times 10^{-13}\ \text{eV} & (n=5/2) \end{cases} \quad (14)$$

for the nonobservation of QD effects for an SN at 10 kpc from Earth. DUNE is not capable of imposing strong bounds in an IH scenario. JUNO performance is improved for distances $\lesssim$1 kpc compared to NH. The results are summarized in Table I in Appendix C.

A 20 kpc SN could not impose strong bounds for individual experiments. Distances as far as 50 kpc (as the

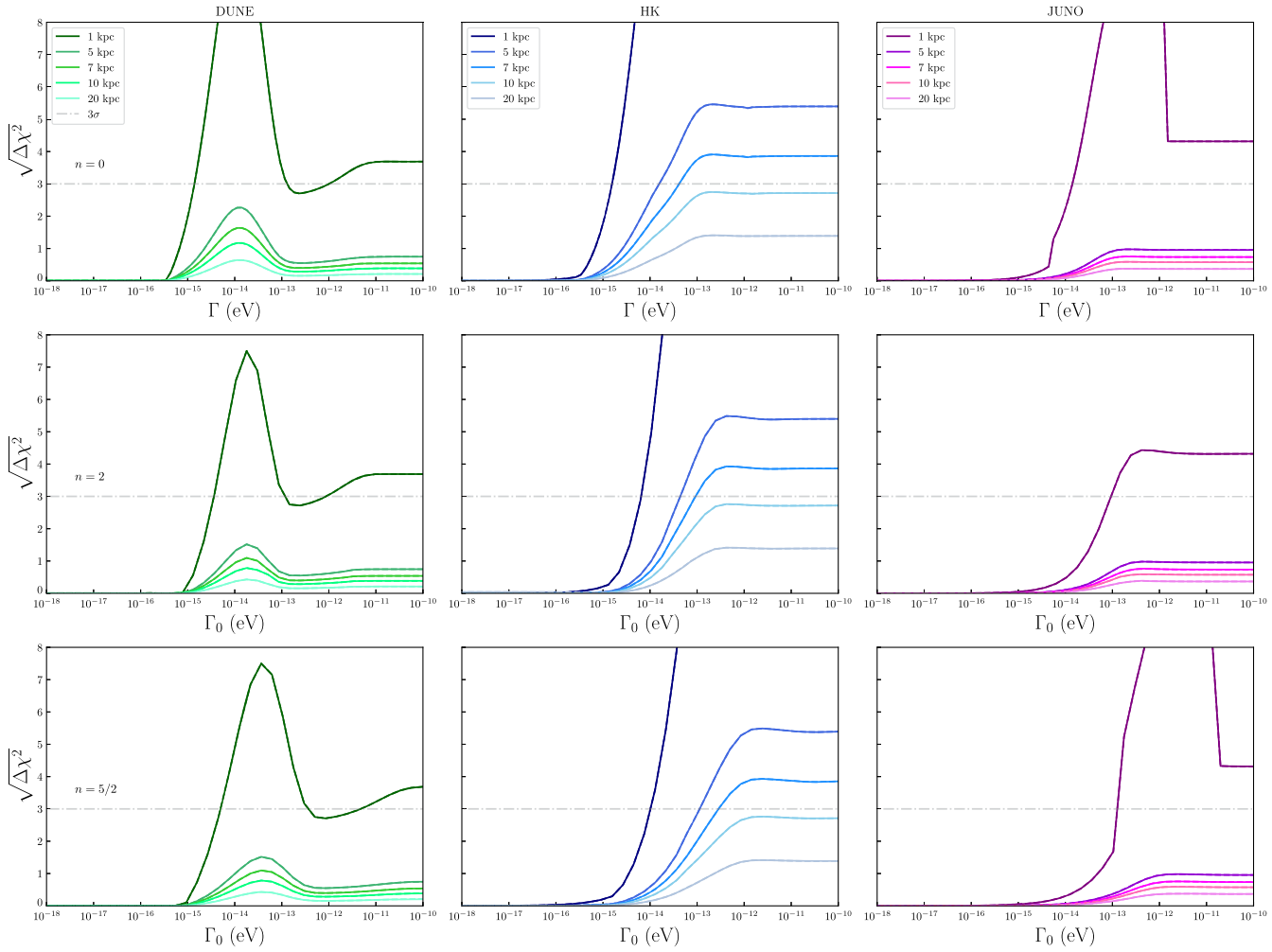

FIG. 13. Same as Fig. 12 but with IH as the true theory, marginalized over the parameters of the IH + QD model.

Large Magellanic Cloud) were not investigated in this work, given the lack of events per bin, in which a more refined unbinned statistical analysis would be required, which is not strongly motivated by the fact that expected limits are below 2σ.

The bounds and sensitivity of each detector in a given hierarchy shown above could be associated with the sensitivity to P_{ee} and $\bar{P}_{ee}$ shown in Fig. 11. In NH (left plot), limits over P_{ee} are more restrictive than $\bar{P}_{ee}$ with respect to maximal mixing represented by the black dot. For IH (right plot), we have an opposite sensitivity, since $P_{ee} \sim 1/3$, while for $\bar{P}_{ee}$ there is a gap between the best fit and $1/3$ probability, allowing limits with certain significance to be imposed. Since DUNE is most sensitive to ν_e, via ν_e-Ar interaction, it will be more sensitive to P_{ee} and then more relevant in the NH scenario. As for HK and JUNO, they are more sensitive to $\bar{\nu}_e$ and therefore to $\bar{P}_{ee}$, which reflects a better performance in the IH scenario. In our calculations, the elastic scattering considered in HK does not contribute much to the total χ^2.

B. MSC$^{\epsilon}$

The same procedure described in the section above was performed on the MSC$^{\epsilon}$ model, with bounds over the parameter Γ_8. The results are summarized in Fig. 14 for NH vs NH + QD. SN distance also plays an important role in this scenario as shown in the relatively large difference in sensitivity for 1 kpc and 10 kpc, with other SN distances in between with intermediate statistical significance with the same plateau pattern of $\sqrt{\Delta\chi^2}$ for higher values of Γ_8, similarly as some of the results for MSC$^{\epsilon}$. DUNE has the best performance for the tested SN distances and even for a 10 kpc SN, bounds with 3σ could be achieved for $n = 0$, 2, and $5/2$. Despite the stronger effects caused by MSC for larger distances, the number of events decreases with L^2, and stronger limits can be imposed for an SN happening at shorter distances, reflecting that the larger number of neutrinos arriving at the detector is a crucial aspect.

From Fig. 14, taking the result of a 10 kpc SN ($27M_{\odot}$), for the nonobservation of QD effects, DUNE would potentially

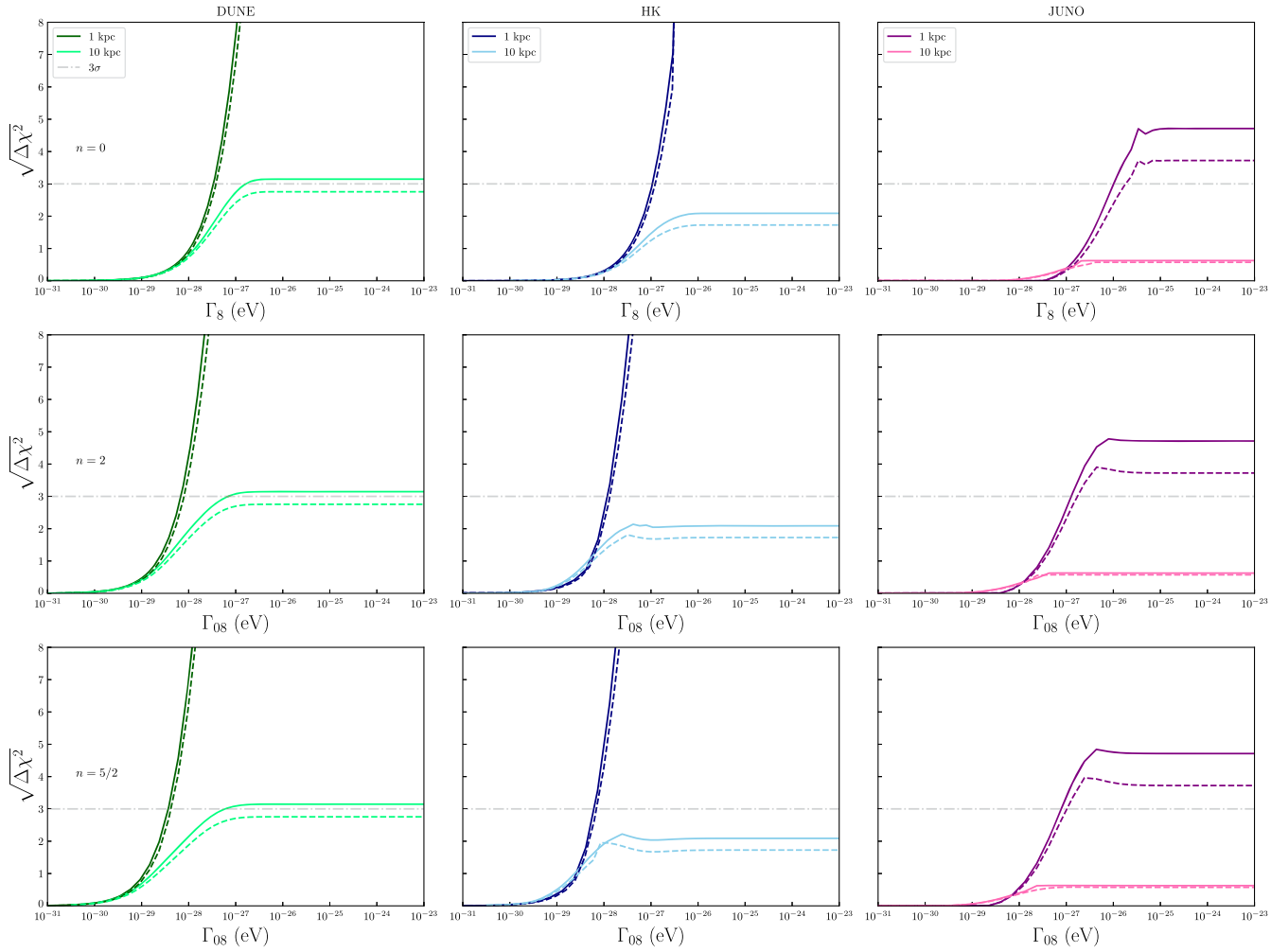

FIG. 14. Same as Fig. 12 but for MSC$^{\epsilon}$ with simulations of the $27M_{\odot}$ (solid) and $11.2M_{\odot}$ (dashed) progenitor masses. The bounds are orders of magnitude more restrictive than for MSC$^{\epsilon}$.

impose $\Gamma_8 \leq 4.2 \times 10^{-28}$ eV for 2σ and $\Gamma_8 \leq 1.7 \times 10^{-27}$ eV for 3σ with $n = 0$, whereas the HK bound is $\Gamma_8 \leq 4.2 \times 10^{-27}$ eV for 2σ. Looking at limits from various works [23,33,35–42,44,45], to the best knowledge of the authors, this is an unprecedented level of sensitivity for testing quantum decoherence, orders of magnitude more restrictive than any other work on the subject. Figure 15 shows bounds from works with different sources and the potential ones established here for a typical future SN detection.

Note that for $n = 2$ and $5/2$ the bounds are over Γ_{08} in $\Gamma_8 = \Gamma_{08}(E/10\ \text{MeV})^n$. For a 10 kpc SN ($27M_{\odot}$), DUNE 3σ bounds reach

$$\Gamma_{08} \leq \begin{cases} 7.0 \times 10^{-28}\ \text{eV} & (n = 2) \\ 6.2 \times 10^{-28}\ \text{eV} & (n = 5/2) \end{cases}. \tag{15}$$

HK is able to achieve 2σ bounds as restrictive as $\Gamma_{08} \leq 2.7 \times 10^{-28}$ eV and $\Gamma_{08} \leq 1.2 \times 10^{-28}$ eV for $n = 2$ and $5/2$ respectively. All mentioned results are summarized in Table II in Appendix C.

We also performed a combined fit for the three detectors using the same ν hierarchy scheme shown in Fig. 16, where a 3σ limit for a 10 kpc SN would reach

$$\Gamma_{08} \leq \begin{cases} 6.2 \times 10^{-28}\ \text{eV} & (n = 0) \\ 1.2 \times 10^{-28}\ \text{eV} & (n = 2) \\ 0.72 \times 10^{-28}\ \text{eV} & (n = 5/2) \end{cases}. \tag{16}$$

Even a 4σ of maximal mixing is possible to be achieved for all values of n, but such significance is achieved only by the $27M_{\odot}$ simulated progenitor. Although a combined analysis reaches high significance, it should be taken with a grain of salt, since it is not possible to be sure that experiments would be simultaneously in operation.

Using the same procedure as done in NH, we make the analysis assuming IH as the true mixing and marginalizing over IH + QD. The results are shown in Fig. 17. HK has the

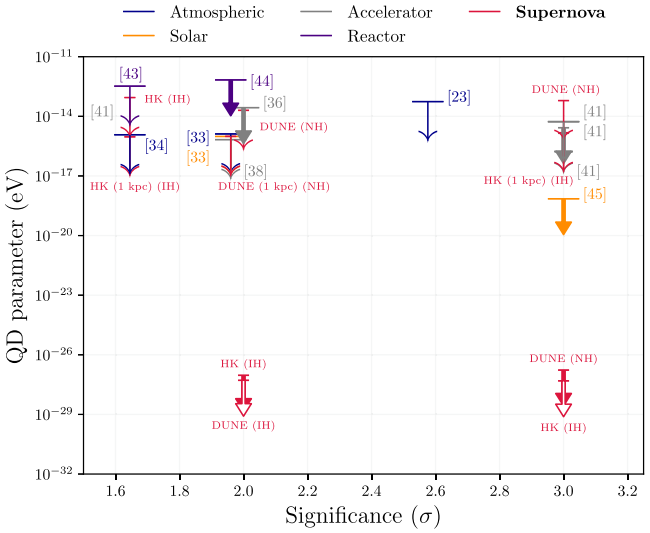

FIG. 15. Current bounds on quantum decoherence for a number of works from many neutrino sources and also the SN limits presented here ($n = 0$). Arrows with longer horizontal bases correspond to current experimental bounds, whereas minor bases are with respect to possible future limits given a nonobservation of QD effects. Numbers in the arrows indicate the reference in which the limits were obtained. Thin arrows indicate bounds equivalent to MSC$^{\not e}$, while thick-filled ones are the MSC^{e}. White-filled thick arrows correspond to ν-loss bounds. Supernova limits described in this work are in red, and are with respect to a distance of 10 kpc from Earth unless distance is indicated, with more restrictive bounds being possible for closer SNs.

strongest bounds on this scenario but does not reach 3σ for a 10 kpc SN, even though the potential limits for 2σ are

$$\Gamma_{08} \lesssim \begin{cases} 1.3 \times 10^{-27}\ \text{eV} & (n = 0) \\ 1.4 \times 10^{-28}\ \text{eV} & (n = 2) \\ 4.9 \times 10^{-28}\ \text{eV} & (n = 5/2) \end{cases} . \qquad (17)$$

DUNE has a very poor performance in this scenario for any distance $\gtrsim$1 kpc. JUNO sensitivity is similar to NH marginalization discussed above. In a combined fit in IH, shown in Fig. 18, the following 3σ limits can be obtained for a 10 kpc SN:

$$\Gamma_{08} \lesssim \begin{cases} 5.4 \times 10^{-27}\ \text{eV} & (n = 0) \\ 3.5 \times 10^{-27}\ \text{eV} & (n = 2) \\ 3.3 \times 10^{-27}\ \text{eV} & (n = 5/2) \end{cases} . \qquad (18)$$

To check the impact of regeneration on the above results, we calculated the potential bounds of a combined detection of DUNE, HK, and JUNO including this effect. We test different θ_z, the zenith with respect to DUNE, with the assumption that the SN flux comes from DUNE longitude. The results are in Fig. 19. We can note in the left plot that the impact of the Earth matter effect is small but enhances possible future bounds on QD for a 10 kpc detection, and limits could be stressed beyond 4σ. The right plot shows the situation where the IH scenario is assumed to be true and NH + QD is marginalized. We will discuss such a scenario in Sec. V, but we also see that regeneration will not significantly change the results.

C. Neutrino loss

Since in ν-loss the spectrum of events decreases asymptotically to zero, the sensitivity on this scenario is expected to be as significant or even more than MSC for all experiments. Since the calculated number of events for NH is low (mainly for DUNE and JUNO) and ν loss would decrease it, not fulfilling our requirement of $\gtrsim$5 events per bin, we perform here only the IH (true) versus IH + QD. Figure 20 shows the $\sqrt{\Delta\chi^2}$ for each individual detector. We see that high values of γ could be strongly bounded, even for JUNO. For an SN from 10 kpc away from Earth, DUNE, HK, and JUNO would be capable to impose $\gamma \leq 5.2 \times 10^{-28}$ eV, $\gamma \leq 4.9 \times 10^{-28}$ eV, and $\gamma \leq 5.9 \times 10^{-28}$ eV respectively with 3σ of significance ($n = 0$). Note that beyond 10 kpc the number of events per bin would be significantly small for a ν-loss scenario, and we do not consider it in this analysis.

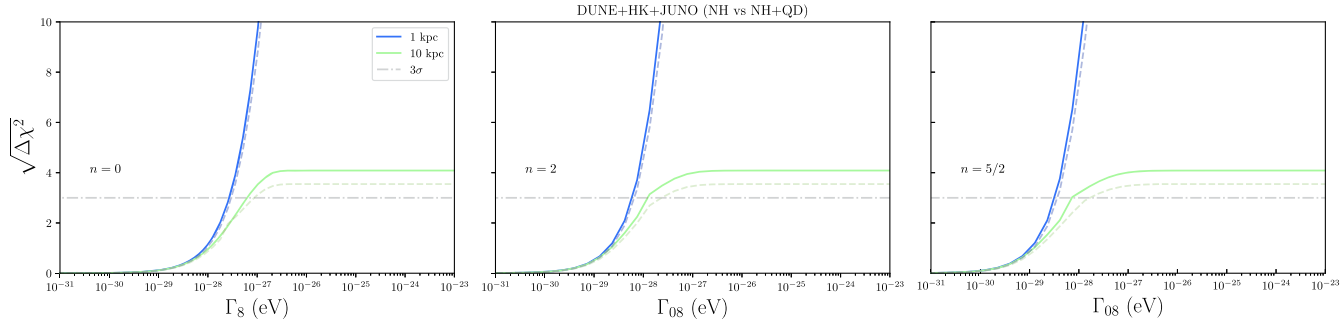

FIG. 16. Combined fit for the true MSW-NH marginalizing over MSW-NH with QD (MSC^{e}) effects.

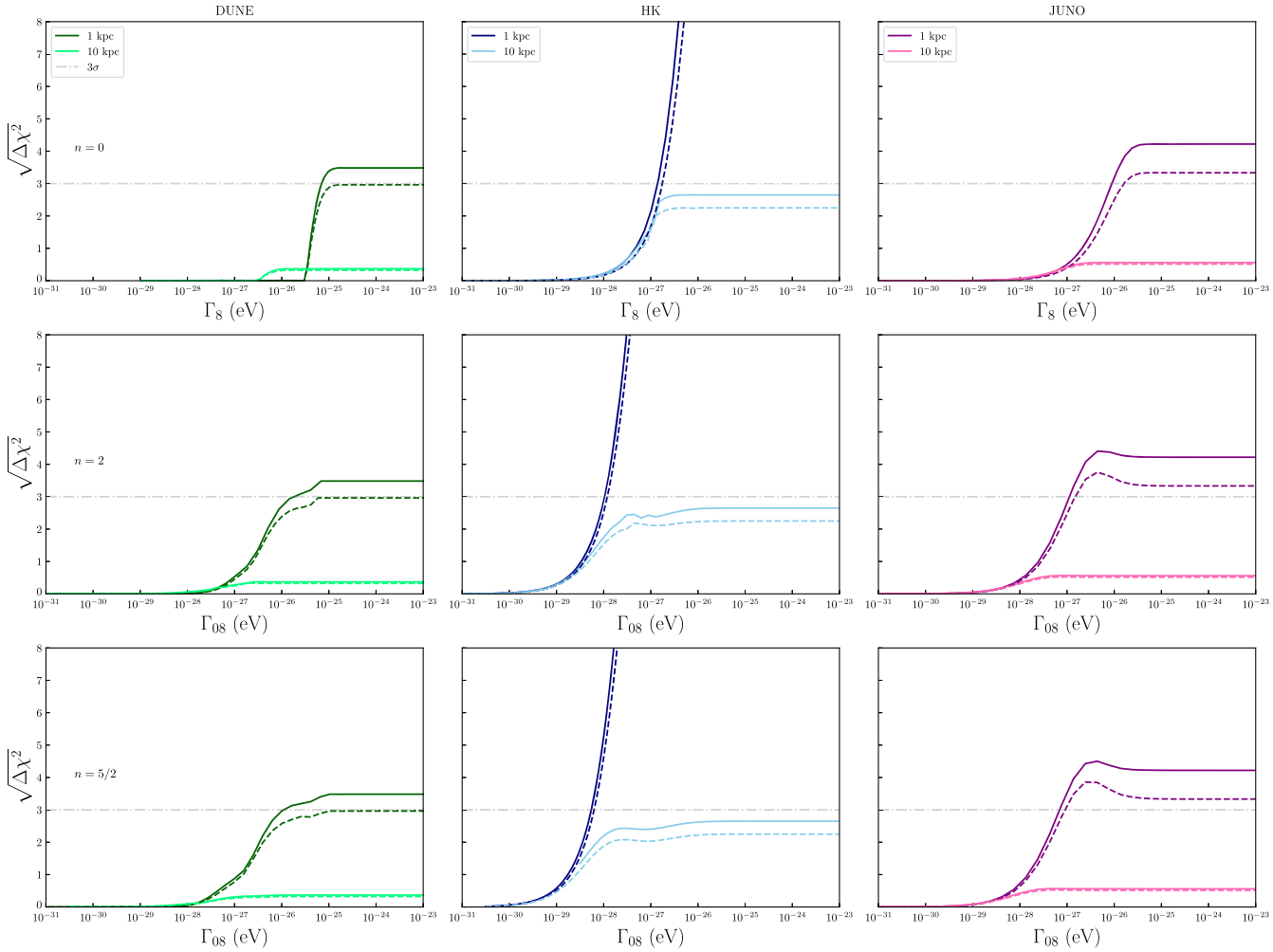

FIG. 17. Same as Fig. 14 but for IH versus IH + QD.

HK is capable to achieve the best (3σ) bounds with $\gamma_0 \leq 2.1 \times 10^{-29}$ eV and $\gamma_0 \leq 1.2 \times 10^{-29}$ eV for $n = 2$ and $5/2$ respectively, with a 10 kpc SN. Although not shown in the plots, it is worth mentioning that HK would impose bounds on γ even for NH, given the high statistics associated with this experiment, being the most sensitive one for the ν-loss model. We summarize the possible future bounds and all mentioned results here in Table III in Appendix C.

V. NEUTRINO MASS HIERARCHY MEASUREMENT

In a future supernova detection, the neutronization burst arises as a robust test of neutrino mass hierarchy, with ν-Ar in DUNE capable of determining the correct scenario with relatively high confidence. However, although possible strong bounds could be imposed on quantum decoherence,

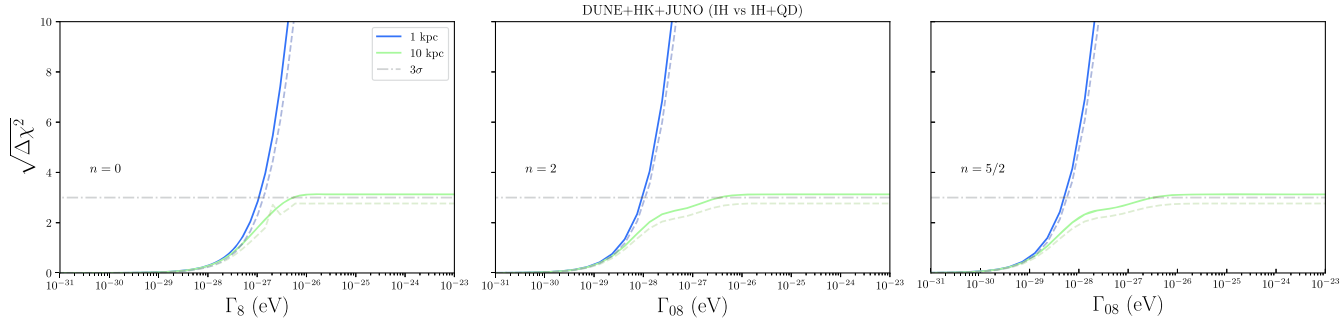

FIG. 18. Same as Fig. 16 but now accounting for the IH scenario.

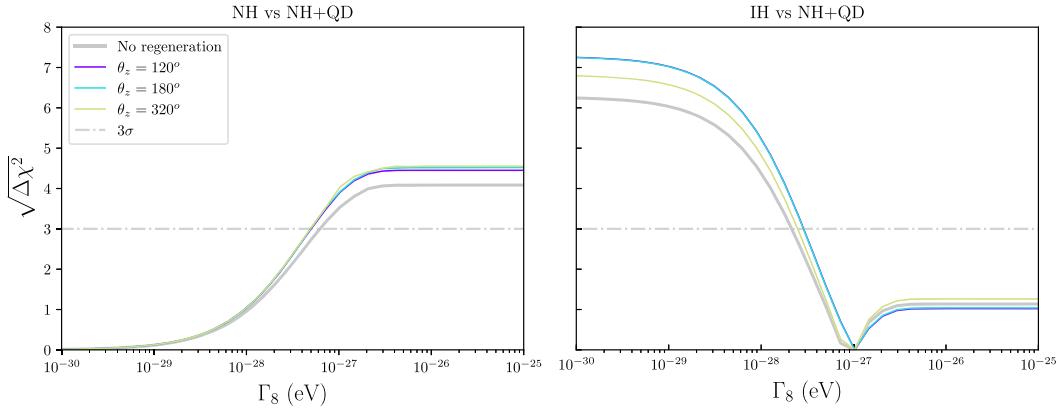

FIG. 19. Limits on MSC with the impact of Earth matter effects for an SN 10 kpc from Earth and the $27M_\odot$ simulation for different zenith angles θ_z ($n = 0$). The limits correspond to a combined detection of DUNE, HK, and JUNO, but θ_z is with respect to DUNE, with SN beam in the direction of DUNE longitude. The $\theta_z = 320°$ means that regeneration effects at HK and JUNO are expected, even if the SN beam does not cross Earth for reaching DUNE.

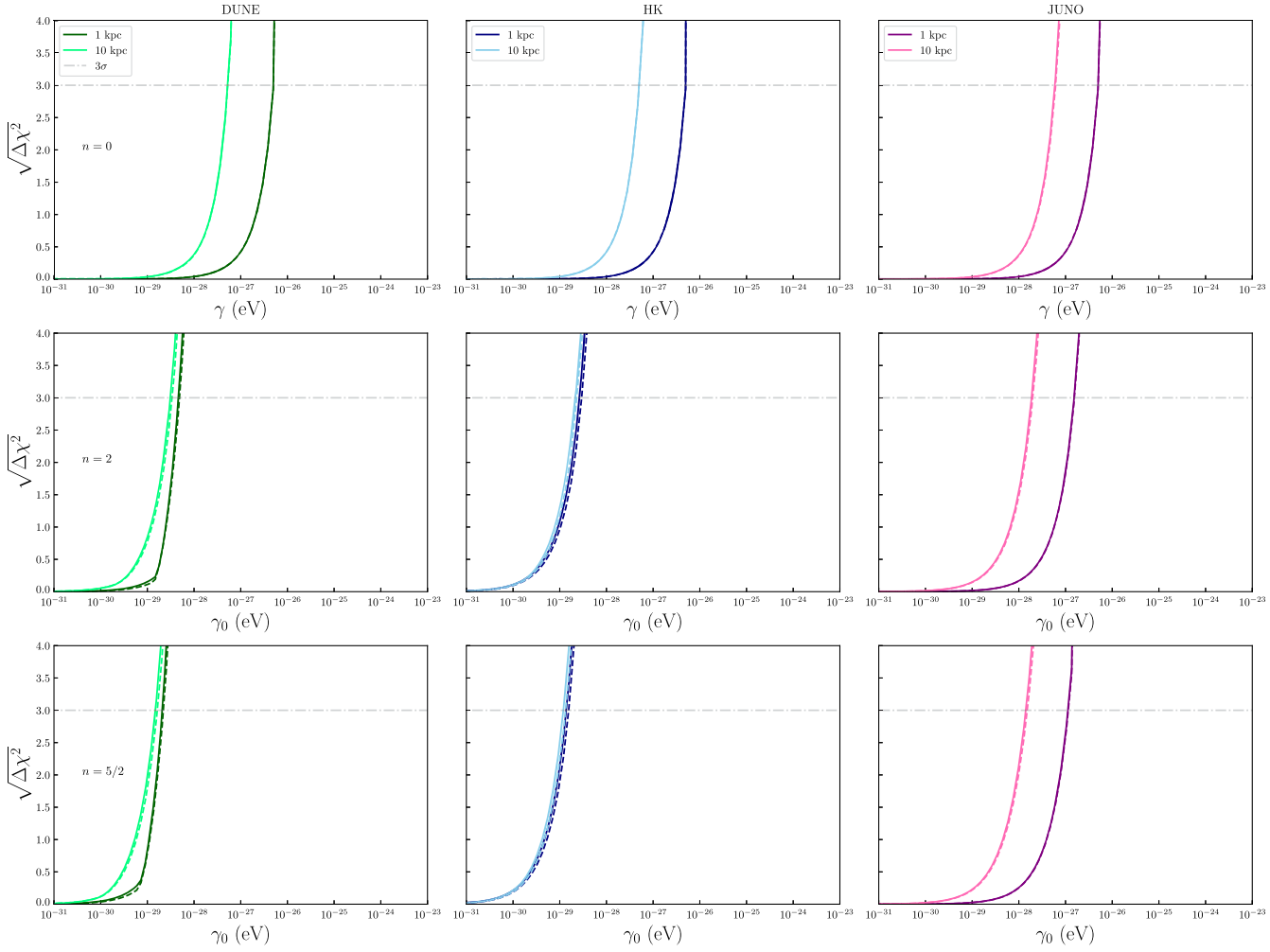

FIG. 20. Limits on γ for a SN at 1 kpc and 10 kpc from Earth for all detectors in the ν-loss scenario with true IH marginalized over the parameters of the IH + QD model.

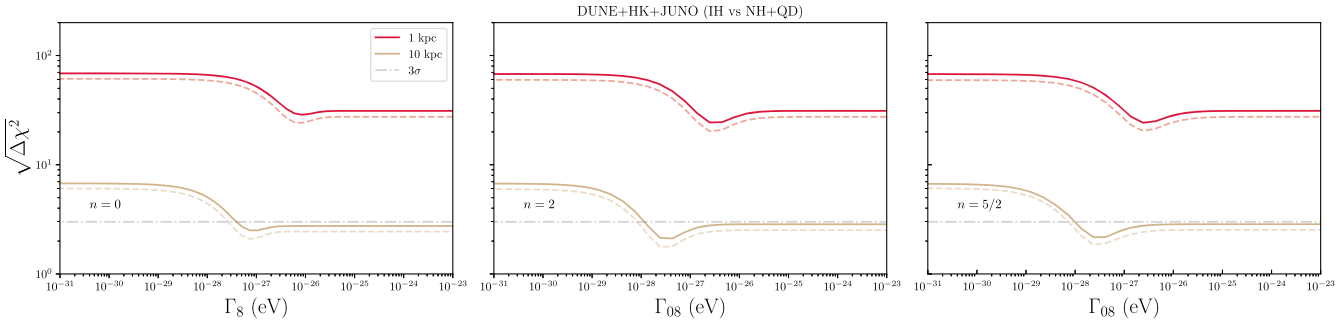

FIG. 21. Statistically comparing the IH to NH with the impact of quantum decoherence for a combined detection using the $11.2M_\odot$ (dashed) and $27M_\odot$ (solid) simulations. No regeneration effects were taken into account.

if QD plays a significant role in ν mixing, the IH could be mimicked by a NH with the impact of QD (particularly, in the MSC models). A similar analysis was performed in the context of ν decay in [68]. Therefore, the question that arises is how much NH and IH are distinguishable if we compare both hierarchies superposing the standard NH to QD. Figure 21 shows the statistical bounds of the scenario where IH is taken as the true theory and NH + QD is marginalized in a combined detection for $n = 0, 2, 5/2$. The results show that the significance of hierarchy determination significantly weakens for the tested SN distances, and even a combined detection could not disentangle the hierarchies if MSC plays an important role.

To check this statement we can compare the values of $\sqrt{\Delta\chi^2}$ for $\Gamma_8 \to 0$ and $\Gamma_8 \to \infty$ in Fig. 21. We can state that $\sqrt{\Delta\chi^2}|_{\Gamma_8\to 0}$ corresponds to the distinguishability of hierarchy in a standard scenario since Γ_8 is small enough to neglect QD effects. The plateau in the limit of $\sqrt{\Delta\chi^2}|_{\Gamma_8\to\infty}$ shows how NH + QD would differ from IH in a future combined detection, in which it has lower values of $\sqrt{\Delta\chi^2}$, resulting in a less significant hierarchy discrimination. Taking as a reference a SN distance of 10 kpc for the $27M_\odot$ simulation, with a combined detection of DUNE, HK, and JUNO, we have a $\sqrt{\Delta\chi^2}|_{\Gamma_8\to 0} = 6.89$ going to $\sqrt{\Delta\chi^2}|_{\Gamma_8\to\infty} = 3.13$. For an individual detection with the same SN distance, DUNE would change from $\sqrt{\Delta\chi^2}|_{\Gamma_8\to 0} = 5.70$, which is statistically significant to determine the hierarchy, to a mere $\sqrt{\Delta\chi^2}|_{\Gamma_8\to\infty} = 0.37$. HK also could be affected with a $\sqrt{\Delta\chi^2}|_{\Gamma_8\to 0} = 3.36$ going to $\sqrt{\Delta\chi^2}|_{\Gamma_8\to\infty} = 2.65$. JUNO can not distinguish the neutrino hierarchies significantly at 10 kpc. It is important to mention that for 1 kpc and 5 kpc DUNE could be highly affected by this hierarchy misidentification, but HK still would provide a distinction of $\gtrsim 5\sigma$ even with QD effects. For SN distances > 5 kpc, the neutrino hierarchies would be hardly disentangled by the tested experiments if QD effects are significant. As far as we tested, the ν-loss model did not lead to the same potential hierarchy misidentification found in the MSC.

VI. CONCLUSIONS

In this paper, we have explored the capability of a future SN neutrino detection in measuring QD effects and potentially imposing limits on QD parameters if quantum decoherence is not observed. As the neutrinos are already treated as an incoherent mixture of mass eigenstates inside the SN, damping effects are not expected; then we explore secondary quantum decoherence scenarios, such as the relaxation mechanism, which can be potentially observed in a SN neutrino signal. We limit ourselves to scenarios where the decoherence matrix $\tilde{D}$ is diagonal in the neutrino vacuum mass basis. Among the possible models to be investigated, we consider the ones we denoted as MSC, leading to maximal mixing of states, and the neutrino loss (ν loss), associated with the loss of neutrino flux along propagation. These scenarios are well-motivated by quantum gravity, where a possible dependency with energy is expected in the form of $\gamma = \gamma_0(E/E_0)^n$, and therefore, we explore possible future limits on the decoherence parameters for different n.

The analysis was done considering DUNE, HK, and JUNO as possible detectors. For the neutrino flux data, three progenitor stars were considered, a $40M_\odot$ (LS180-s40.0), $27M_\odot$ (LS220s27.0c), and $11.2M_\odot$ (LS220s11.2c), using the SN simulation data from the Garching group [7,10,57]. To get around the unsolved problem of neutrino collective effects, only the neutronization burst was considered, given that collective effects are expected to not play a significant role in this emission phase.

When considering the neutrino propagation inside the supernova, the relaxation effect could affect the neutrino flavor conversion, even with the assumption of no exchange of neutrino energy to the environment, or $[H, V_p] = 0$ (MSC^e). We show that in this regime it is possible to get competitive limits to QD parameters with a future SN detection. However, the required values for the decoherence parameters need to be much larger than the ones in the scenario where $[H, V_p] \neq 0$ (MSC$^\epsilon$) (see Appendix B), which would provide the most restrictive bounds on QD. For MSC$^\epsilon$, we only consider the decoherence/relaxation acting on neutrino propagation in

the vacuum from the SN until it reaches the detectors at Earth, for which the propagation length is orders of magnitude larger than the SN size, and therefore, more sensitive to the relaxation effects. We also explore the possible effects of Earth regeneration due to the neutrino propagation inside the Earth, which has minor effects in the bounds for the relaxation parameters, the vacuum propagation being the most relevant coherence length.

With all considerations, we show that the detectors used in the analysis are capable to achieve the limits listed in Tables I and II in Appendix C for the MSC scenario, depending on the distance being considered and the neutrino mass hierarchy. For the NH, the DUNE detector is the most promising one, while HK is the most sensitive in the case of IH. The possible limits on the decoherence parameters are orders of magnitude stronger than the ones imposed by current terrestrial and solar experiments, as shown in Fig. 15. For the ν-loss scenario, the limits are shown in Table III in Appendix C. Owing to the neutrino disappearance, extra care needed to be taken in this scenario so that the requirement of at least five events per bin is fulfilled and the χ^2 analysis can be applied.

Finally, we explored the possible degeneracy between the different standard scenarios of unknown mass hierarchy (NH and IH) without QD and the ones with QD effects included. As we saw, the IH scenario could be easily mimicked by NH combined with QD-MSC effects.

ACKNOWLEDGMENTS

We thank Hans-Thomas Janka and the Garching group for providing the SN simulations used in this work. M. V. S. is thankful to Alberto Gago for pointing out complete positivity relations. E. K. is very grateful for the hospitality of GSSI during the preparation of this manuscript. This study was financed by the Coordenação de Aperfeiçoamento de Pessoal de Nível Superior—Brasil (CAPES)—Finance Code 001, and partially by the Fundação de Amparo à Pesquisa do Estado de São Paulo (FAPESP) Grants No. 2019/08956-2, No. 14/19164-6, and No. 2022/01568-0.

APPENDIX A: HAMILTONIAN PART OF THE EVOLUTION EQUATION

The Hamiltonian part $\tilde{H}$ of $\mathcal{L} = -2(\tilde{H} + \tilde{D})$ operator in Eq. (2) is found in the same way as $\tilde{D}$. The procedure to derive it is expanding operators in $-i[H,\rho]$ in Gell-Mann matrices λ_a, i.e., $H = \sum_a h_a\lambda_a$ and $\rho = \sum_a \rho_a\lambda_a$ for a from 0 to 8, and requiring ρ to be a column vector $|\rho\rangle$ with dimension 9×1, consequently leading to a 9×9 Hamiltonian term that can be written as

$$\tilde{H} = \frac{1}{2}\begin{pmatrix}
0 & 0 & 0 & 0 & 0 & 0 & 0 & 0 & 0\\
0 & 0 & 2h_3 & -2h_2 & h_7 & -h_6 & h_5 & -h_4 & 0\\
0 & -2h_3 & 0 & 2h_1 & h_6 & h_7 & -h_4 & -h_5 & 0\\
0 & 2h_2 & -2h_1 & 0 & h_5 & -h_4 & -h_7 & h_6 & 0\\
0 & -h_7 & -h_6 & -h_5 & 0 & h_3+\sqrt{3}h_8 & h_2 & h_1 & -\sqrt{3}h_5\\
0 & h_6 & -h_7 & h_4 & -h_3-\sqrt{3}h_8 & 0 & -h_1 & h_2 & \sqrt{3}h_4\\
0 & -h_5 & h_4 & h_7 & -h_2 & h_1 & 0 & -h_3+\sqrt{3}h_8 & -\sqrt{3}h_7\\
0 & h_4 & h_5 & -h_6 & -h_1 & -h_2 & h_3-\sqrt{3}h_8 & 0 & \sqrt{3}h_6\\
0 & 0 & 0 & 0 & \sqrt{3}h_5 & -\sqrt{3}h_4 & \sqrt{3}h_7 & -\sqrt{3}h_6 & 0
\end{pmatrix}. \tag{A1}$$

APPENDIX B: DECOHERENCE INSIDE THE SN AND MATTER EFFECTS

The neutrino Hamiltonian in flavor basis affected by the charged current potential V_W, i.e., $H_f = H_f^{\rm vac} + V_W$, can be diagonalized to H_m by a unitary transformation provided by U_m as

$$\rho_f = U_m\rho_m U_m^\dagger \qquad H_f = U_m H_m U_m^\dagger, \tag{B1}$$

getting the most general form of (1) in the effective neutrino mass basis in matter

$$\frac{d\rho_m}{dt} = -i[H_m,\rho_m] - [U_m^\dagger\dot{U}_m,\rho_m] + \sum_p^{N^2-1}\left(V_{pm}\rho_m V_{pm} - \frac{1}{2}\{V_{pm}^2,\rho_m\}\right) \tag{B2}$$

or following the notation in (2)

$$|\dot{\rho}_m\rangle = -2\mathcal{L}_m(t)|\rho_m\rangle. \tag{B3}$$

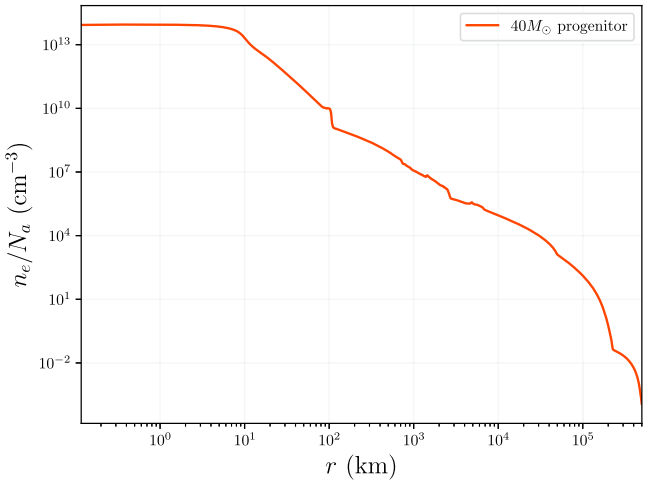

FIG. 22. Snapshot (at 27 ms after the core bounce) of simulated SN electron density profile from the $40M_\odot$ progenitor mentioned in the text [10,57].

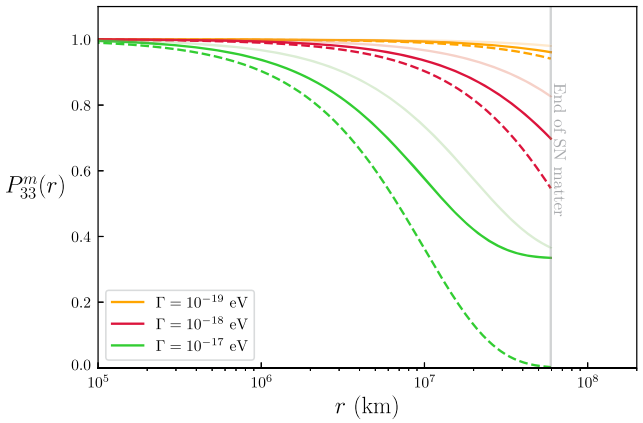

FIG. 23. Solution for a survival probability of mass state 3 along a SN radius for the MSC$^\epsilon$ (solid opaque line) and neutrino loss (dashed). The transparent line shows the same probability but in vacuum. More details about these models are in the text. As it will be clear in our results, even with enhancement of the conversion in matter, values of $\Gamma \sim 10^{-19}$ eV are far higher than the sensitivity of a future SN detection compared to coherence length in vacuum used in the MSC$^\epsilon$ model.

For all purposes of this work, the propagation is adiabatic, or $\dot{U}_m = 0$ in (B2).

We are interested in solving Eq. (B3) in a variable matter density in order to get transition probabilities $P^{m(\mathrm{SN})}_{ij}$ and $\bar{P}^{m(\mathrm{SN})}_{ij}$. It is straightforward to obtain $|\rho\rangle$ in (1), but in the case of $|\rho_m\rangle$, V_{pm} and H_m are time dependent, and the solution is a time-ordered exponential:

$$\mathcal{T}\left\{e^{-2\int_{t_0}^{t} dt' \mathcal{L}_m(t')}\right\} = 1 + (-2)\int_{t_0}^{t} dt_1 \mathcal{L}_m(t_1) + (-2)^2 \int_{t_0}^{t} dt_1 \int_{t_0}^{t_1} dt_2 \mathcal{L}_m(t_1)\mathcal{L}_m(t_2) + \cdots. \quad \text{(B4)}$$

Analytical solutions for specific cases in a variable matter density can be found in [33,69]. However, instead of using a cumbersome approximated approach, we analyze the neutrino evolution into the SN making the limits in the integrals in (B4) $\Delta t = t_n - t_{n-1} \to 0$, allowing one to solve (B4) numerically through the slab approach, i.e., we divided the SN matter density profile into small parts, in which the neutrino Hamiltonian is approximately constant, then we make the time evolution from each step to another until the neutrino reach the vacuum. We use the simulated density profile in Fig. 22 to perform this calculation.

In Fig. 23 we compare the $P^{m(\mathrm{SN})}_{33}$ to the same probability in mass basis in vacuum, which is shown as an enhancement of the deviation from the standard expectation of $P^{m(\mathrm{SN})}_{33} = 1$. In Fig. 2 we show the numerical probabilities of MSC$^\epsilon$ for the mass state in matter solved as described above.

APPENDIX C: TABLES WITH QD BOUNDS

TABLE I. Constraints on Γ from MSC$^\epsilon$ based on the nonobservation of QD effects for the possible neutrino mass hierarchies. The values correspond to 90%(2σ) C.L. in units of $\Gamma \times 10^{-15}$ (eV). For $n \neq 0$ a representative energy of $E_0 = 10$ MeV was chosen, and QD parameters are in eV scale. Values are corresponding to the simulated progenitor of $40M_\odot$.

		NH			IH		
Detector	SN distance	$n = 0$	$n = 2$	$n = 5/2$	$n = 0$	$n = 2$	$n = 5/2$
DUNE	1 kpc	0.89(1.1)	0.76(0.89)	0.65(0.87)	0.88(1.0)	2.5(8.8)	3.2(15)
	5 kpc	5.4(7.0)	4.4(5.9)	6.3(8.7)			
	7 kpc	8.3(11)	7.0(9.4)	11(16)			
	10 kpc	14(20)	12(17)	22(35)			
HK	1 kpc	0.96(1.1)	3.7(4.1)	5.0(5.8)	0.93(1.1)	3.9(4.3)	5.3(6.5)
	5 kpc	4.3(5.7)	16(21)	33(47)	4.9(6.6)	18(23)	38(49)
	7 kpc	7.1(11)	27(38)	53(87)	8.5(13)	28(38)	67(99)
	10 kpc	16(51)	65(120)	150(400)	20(36)	52(80)	140(240)
JUNO	1 kpc	4.2(5.4)	15(19)	30(41)	7.2(8.9)	38(51)	100(180)

TABLE II. Same as Table I but for MSC^e scenario with $2\sigma(3\sigma)$ C.L. in units of $\Gamma_8 \times 10^{-28}$ (eV). The representative energy of $E_0 = 10$ MeV was taken for $n \neq 0$, and QD parameters are in eV scale. Values are corresponding to the simulated progenitor of $27M_\odot$.

		NH			IH		
Detector	SN distance	$n = 0$	$n = 2$	$n = 5/2$	$n = 0$	$n = 2$	$n = 5/2$
DUNE	1 kpc	2.1(3.3)	0.43(0.67)	0.24(0.37)	490(700)	50(180)	33(110)
	5 kpc	2.8(5.2)	0.58(1.1)	0.34(0.75)			
	7 kpc	3.2(7.1)	0.71(1.9)	0.46(1.4)			
	10 kpc	4.2(17)	1.1(7.0)	0.80(6.1)			
HK	1 kpc	6.8(11)	0.81(1.1)	0.43(0.58)	9.2(14)	0.68(1.0)	0.36(0.54)
	5 kpc	9.6(23)	0.92(1.9)	0.48(1.0)	10(18)	0.80(1.5)	0.44(0.82)
	7 kpc	13	1.2	0.61(2.6)	11(25)	0.94(2.5)	0.51(1.4)
	10 kpc	42	2.7	1.2	13	1.4	4.9
JUNO	1 kpc	51(100)	6.4(13)	4.0(7.8)	47(89)	5.6(11)	3.5(6.9)

TABLE III. Same as Tables I and II but for ν-loss scenario, with 3σ bounds over $\gamma \times 10^{-29}$ (eV).

		IH		
Detector	SN distance	$n = 0$	$n = 2$	$n = 5/2$
DUNE	1 kpc	500	4.6	2.1
	5 kpc	100	3.3	1.6
	7 kpc	74	3.2	1.5
	10 kpc	52	3.1	1.5
HK	1 kpc	500	2.6	1.4
	5 kpc	100	2.3	1.2
	7 kpc	70	2.2	1.2
	10 kpc	49	2.1	1.2
JUNO	1 kpc	500	150	110
	5 kpc	100	32	24
	7 kpc	78	24	18
	10 kpc	59	19	14

[1] K. Rozwadowska, F. Vissani, and E. Cappellaro, New Astron. **83**, 101498 (2021).

[2] R. Acciarri, M. Acero, M. Adamowski, C. Adams, P. Adamson, S. Adhikari, Z. Ahmad, C. Albright, T. Alion, E. Amador *et al.*, arXiv:1601.02984.

[3] B. Abi, R. Acciarri, M. Acero, M. Adamowski, C. Adams, D. Adams, P. Adamson, M. Adinolfi, Z. Ahmad, C. Albright *et al.*, arXiv:1807.10334.

[4] B. Abi, R. Acciarri, M. A. Acero, G. Adamov, D. Adams, M. Adinolfi, Z. Ahmad, J. Ahmed, T. Alion, S. Alonso Monsalve *et al.*, Eur. Phys. J. C **81**, 423 (2021).

[5] K. Abe, K. Abe, H. Aihara, A. Aimi, R. Akutsu, C. Andreopoulos, I. Anghel, L. Anthony, M. Antonova, Y. Ashida *et al.*, arXiv:1805.04163.

[6] F. An, G. An, Q. An, V. Antonelli, E. Baussan, J. Beacom, L. Bezrukov, S. Blyth, R. Brugnera, M. B. Avanzini *et al.*, J. Phys. G **43**, 030401 (2016).

[7] A. Mirizzi, I. Tamborra, H.-T. Janka, N. Saviano, K. Scholberg, R. Bollig, L. Hüdepohl, and S. Chakraborty, Riv. Nuovo Cimento Soc. Ital. Fis. **39**, 1 (2016).

[8] I. Tamborra, L. Hüdepohl, G. G. Raffelt, and H.-T. Janka, Astrophys. J. **839**, 132 (2017).

[9] B. Müller, T. Melson, A. Heger, and H.-T. Janka, Mon. Not. R. Astron. Soc. **472**, 491 (2017).

[10] A variety of sophisticated supernovae simulations from 1 to 3D is done by the Garching group and access to specific results can be found at https://wwwmpa.mpa-garching.mpg.de/ccsnarchive/ (2022).

[11] I. Tamborra and S. Shalgar, Annu. Rev. Nucl. Part. Sci. **71**, 165 (2021).

[12] J. Kersten and A. Y. Smirnov, Eur. Phys. J. C **76**, 1 (2016).

[13] E. Akhmedov, J. Kopp, and M. Lindner, J. Cosmol. Astropart. Phys. 09 (2017) 017.

[14] E. Akhmedov and A. Y. Smirnov, J. High Energy Phys. 11 (2022) 082.
[15] T. Ohlsson, Phys. Lett. B **502**, 159 (2001).
[16] S. W. Hawking, in *Euclidean Quantum Gravity* (World Scientific, Singapore, 1975), pp. 167–188.
[17] J. D. Bekenstein, Phys. Rev. D **12**, 3077 (1975).
[18] S. W. Hawking, Commun. Math. Phys. **87**, 395 (1982).
[19] J. Ellis, J. S. Hagelin, D. V. Nanopoulos, and M. Srednicki, Nucl. Phys. **B241**, 381 (1984).
[20] R. M. Wald, *Quantum Field Theory in Curved Spacetime and Black Hole Thermodynamics* (University of Chicago Press, Chicago, 1994).
[21] W. G. Unruh and R. M. Wald, Phys. Rev. D **52**, 2176 (1995).
[22] J. Ellis, N. Mavromatos, and D. Nanopoulos, Chaos, Solitons Fractals **10**, 345 (1999).
[23] E. Lisi, A. Marrone, and D. Montanino, Phys. Rev. Lett. **85**, 1166 (2000).
[24] J. Alexandre, K. Farakos, N. E. Mavromatos, and P. Pasipoularides, Phys. Rev. D **77**, 105001 (2008).
[25] N. E. Mavromatos, J. Phys. Conf. Ser. **171**, 012007 (2009).
[26] M. Dvornikov, Phys. Rev. D **100**, 096014 (2019).
[27] T. Stuttard and M. Jensen, Phys. Rev. D **102**, 115003 (2020).
[28] G. G. Luciano and M. Blasone, Universe **7**, 417 (2021).
[29] T. Stuttard, Phys. Rev. D **104**, 056007 (2021).
[30] D. Hellmann, H. Päs, and E. Rani, Phys. Rev. D **106**, 083013 (2022).
[31] D. Hellmann, H. Päs, and E. Rani, Phys. Rev. D **105**, 055007 (2022).
[32] M. M. Ettefaghi, R. R. Arani, and Z. T. Lotfi, Phys. Rev. D **105**, 095024 (2022).
[33] P. Coloma, J. Lopez-Pavon, I. Martinez-Soler, and H. Nunokawa, Eur. Phys. J. C **78**, 1 (2018).
[34] R. Abbasi, M. Ackermann, J. Adams, S. Agarwalla, J. Aguilar, M. Ahlers, J. Alameddine, N. Amin, K. Andeen, G. Anton *et al.*, arXiv:2308.00105.
[35] Y. Farzan, T. Schwetz, and A. Y. Smirnov, J. High Energy Phys. 07 (2008) 067.
[36] R. L. N. Oliveira, M. M. Guzzo, and P. C. de Holanda, Phys. Rev. D **89**, 053002 (2014).
[37] R. L. Oliveira, Eur. Phys. J. C **76**, 1 (2016).
[38] J. A. B. Coelho, W. A. Mann, and S. S. Bashar, Phys. Rev. Lett. **118**, 221801 (2017).
[39] J. A. Coelho and W. A. Mann, Phys. Rev. D **96**, 093009 (2017).
[40] J. Carrasco, F. Díaz, and A. Gago, Phys. Rev. D **99**, 075022 (2019).
[41] J. Carpio, E. Massoni, and A. Gago, Phys. Rev. D **100**, 015035 (2019).
[42] G. B. Gomes, D. Forero, M. M. Guzzo, P. C. de Holanda, and R. Oliveira, Phys. Rev. D **100**, 055023 (2019).
[43] V. D. Romeri, C. Giunti, T. Stuttard, and C. A. Ternes, J. High Energy Phys. 09 (2023) 097.
[44] G. B. Gomes, M. Guzzo, P. De Holanda, and R. Oliveira, Phys. Rev. D **95**, 113005 (2017).
[45] P. C. de Holanda, J. Cosmol. Astropart. Phys. 03 (2020) 012.
[46] Y. Farzan and T. Schwetz, arXiv:2306.09422.
[47] V. Gorini, A. Kossakowski, and E. C. G. Sudarshan, J. Math. Phys. (N.Y.) **17**, 821 (1976).
[48] G. Lindblad, Commun. Math. Phys. **48**, 119 (1976).
[49] F. Benatti and H. Narnhofer, Lett. Math. Phys. **15**, 325 (1988).
[50] J. F. Nieves and S. Sahu, Phys. Rev. D **100**, 115049 (2019).
[51] J. F. Nieves and S. Sahu, Phys. Rev. D **102**, 056007 (2020).
[52] F. Benatti and R. Floreanini, Nucl. Phys. **B488**, 335 (1997).
[53] F. Benatti and R. Floreanini, J. High Energy Phys. 02 (2000) 032.
[54] R. Oliveira and M. Guzzo, Eur. Phys. J. C **69**, 493 (2010).
[55] G. Amelino-Camelia, Living Rev. Relativity **16**, 1 (2013).
[56] L. A. Anchordoqui, H. Goldberg, M. C. Gonzalez-Garcia, F. Halzen, D. Hooper, S. Sarkar, and T. J. Weiler, Phys. Rev. D **72**, 065019 (2005).
[57] P. D. Serpico, S. Chakraborty, T. Fischer, L. Hüdepohl, H.-T. Janka, and A. Mirizzi, Phys. Rev. D **85**, 085031 (2012).
[58] J. Collaboration *et al.*, Prog. Part. Nucl. Phys. **123**, 103927 (2022).
[59] P. Vogel and J. F. Beacom, Phys. Rev. D **60**, 053003 (1999).
[60] K. Scholberg, J. B. Albert, and J. Vasel, Astrophys. Source Code Library, ascl (2021), https://ui.adsabs.harvard.edu/abs/2021ascl.soft09019S.
[61] A. de Gouvêa, P. A. Machado, Y. F. Perez-Gonzalez, and Z. Tabrizi, Phys. Rev. Lett. **125**, 051803 (2020).
[62] A. S. Dighe and A. Yu. Smirnov, Phys. Rev. D **62**, 033007 (2000).
[63] F. Pompa, F. Capozzi, O. Mena, and M. Sorel, Phys. Rev. Lett. **129**, 121802 (2022).
[64] D. L. Anderson, *Theory of the Earth* (Blackwell Scientific Publications, Boston, MA, 1989).
[65] G. L. Fogli, E. Lisi, A. Marrone, D. Montanino, and A. Palazzo, Phys. Rev. D **66**, 053010 (2002).
[66] A. de Gouvêa, I. Martinez-Soler, and M. Sen, Phys. Rev. D **101**, 043013 (2020).
[67] P. Dedin Neto, M. V. dos Santos, P. C. de Holanda, and E. Kemp, Eur. Phys. J. C **83**, 459 (2023).
[68] E. A. Delgado, H. Nunokawa, and A. A. Quiroga, J. Cosmol. Astropart. Phys. 01 (2022) 003.
[69] F. Benatti and R. Floreanini, Phys. Rev. D **71**, 013003 (2005).